Application of Probabilistic Modelling to the Lifetime Management of Nuclear Boilers in the Creep Regime: Part 2

by R.A.W.Bradford[1] and P.J.Holt[2]
[1]EDF Energy, Barnett Way, Barnwood, Glos.GL4 3RS, rick.bradford@edf-energy.com
[2]Veritan Ltd, 4 Valley View, Lower Mills, Stonehouse, Glos.GL10 2BB, peter.holt@veritan.co.uk

Abstract

Monte Carlo probabilistic simulation has been applied to a large population of nominally identical components in an AGR boiler operating in the creep regime. Some of the components have a history of partial steam flow restrictions which can cause an elevation of their operating temperature, potentially raising the rate of creep life usage. Metal losses due to steam-side and gas-side oxidation and chemical cleaning operations can also exacerbate the rate of creep life usage. The R5 procedure has been used within a probabilistic program to calculate the expected frequency of both creep rupture and creep-fatigue crack initiation. The probabilistic approach is shown to provide a better quantitative guide to the commercial threat than traditional deterministic methodologies based on bounding data. In particular, probabilistic assessments identify the parameters which most significantly influence plant life.

Keywords

Rupture, Creep-fatigue, Crack Initiation, Boiler, Monte Carlo, Probabilistic, Lifetime

1. Introduction

Some of the UK's Advanced Gas Cooled (AGR) reactors are already operating beyond their original design lifetime, and all the AGRs may be expected to do so in due course. At full power the reactor coolant gas temperature is around 650^{o}C as it enters the boilers. Consequently, creep is a potentially life limiting mechanism for some boiler components. The accurate prediction of creep lives is hampered by the large scatter in creep material properties, the uncertainties in stressing and operating conditions, and the sparsity of, or uncertainties in, inspection information. For the purposes of underwriting nuclear safety, bounding assumptions ensure conservative assessments. However, the degree of conservatism in such deterministic assessments can be such that, whilst entirely appropriate for ensuring safety, they give no realistic picture of plant lifetimes.

In common with boilers in conventional power plant, the boiler surfaces in AGRs consist of large numbers of very similar tubes and associated features. This lends itself naturally to a probabilistic treatment. The cracking or failure of small numbers of tubes is tolerable from the nuclear safety perspective. Indeed the occasional occurrence of steam leaks is anticipated and managed, generally by plugging tubes if access difficulties prevent repair. This need have no commercial or safety implications so long as the rate of leaks and the number of tubes requiring plugging remains small. Part 1 of this work, Ref.[1], identified two cases which differ according to the availability of inspection evidence,

(1) Extensive in-service inspection evidence exists and there is a history of cracking as well as some steam leaks;

(2) Little or no in-service inspection evidence exists and hence the potential defectiveness is unknown other than indirectly from a few steam leaks.

Case (1) was addressed in Part 1, Ref.[1]. In that paper the focus was on the probabilistic modelling of crack growth and the probabilistic treatment of inspection

data. The present paper addresses (2). The focus in this case is on probabilistic assessments of an initially defect-free component. Both creep rupture and the initiation of cracking by creep-fatigue have been considered. Like Ref.[1], the R5 procedure, Ref.[2], provides the deterministic methodology at the core of the probabilistic treatment.

A Monte Carlo method is used here to implement the probabilistic assessment. Monte Carlo methods involve randomly sampling the distributed input variables many times so as to build a statistical picture of the output quantities, see for example Ref.[3]. The method has a very wide range of applicability, engineering applications being only one. The method is particularly appropriate when there are a large number of independent variables which can influence the outcome. The Monte Carlo method is being used increasingly in structural integrity applications. Examples include applications to the analysis of creep data or the development of models of creep behaviour, e.g., Refs.[4-10], and applications to lifetime assessment of plant components, both at low temperature, e.g., Refs.[11,12], and within the creep regime, e.g., Refs.[13-19].

It is natural to deploy probabilistic techniques when creep is significant, as a means of addressing the large scatter in creep data, and it is upon this aspect that many papers concentrate. However, the advantage of applying probabilistic techniques to real power plant assessments is that the considerable uncertainty in many other aspects can also be addressed. In Ref.[1], for example, the variability in non-destructive inspection results was found to be the dominant issue. In the present work, uncertainties in operating temperature, loading and tube wall thickness losses all compete with the uncertainties in materials properties for dominance. The present work is relatively unusual in addressing all these issues probabilistically (although the recent work of Huang et al, Ref.[19], is perhaps comparable). It is becoming clear that one of the key benefits of the probabilistic approach is the identification of the factors which are most important. It is anticipated that probabilistic techniques will be used increasingly to support AGR life extensions.

Within the nuclear industry, work of nuclear safety or major commercial significance is subject to independent verification. This presents particular issues for Monte Carlo assessments since these are intrinsically difficult to check ‘by hand’. Consequently the approach taken here was for the two authors, working independently, to produce their own Monte Carlo codes as a cross-check on the final results. Inevitably such independent working leads to many differences in the detailed implementation. Where relevant these differences are alluded to in the paper.

2. Component Modelled

2.1 Boiler Design

Each reactor in question here has 8 boiler units (referred to as ‘pods’), the boiler tubes being of helical design. In the austenitic section at the top of the main boiler (the secondary superheater) the tubes are finned, see Fig.1. There are 19 rows of tubes in each superheater boiler pod, each row being at a different radius and also having a different helical pitch so as to ensure that all tubes have the same length. In general two boiler tube helices are connected together at the top of the boiler by a feature called a bifurcation, Fig.1. A single tailpipe then conveys the steam from the bifurcation to the superheater outlet header. In a few cases, steam from only one boiler tube helix is conveyed to a tailpipe, via a so-called ‘mono-bifurcation’ (the

genuine bifurcations being referred to as ‘dual’). The number of bifurcations per row varies from 3 for the innermost row to 12 for the outermost row. The total number of bifurcations per pod is 147, of which 9 are ‘monos’. Hence the total number of boiler tubes per pod is 285 making 2280 tubes per reactor.

2.2 Tube/Bifurcation Inlet Stub Dimensions

Nominal drawing start-of-life mean dimensions are a bore of ~14mm and thicknesses, ignoring the tube fins, of ~1.8mm (bifurcation inlet) or ~2.0mm (boiler tube). However, the probabilistic code uses distributions of initial dimensions based on drawing tolerances. One code used separate normal distributions for the inner and outer radii with standard deviations ~0.025mm (or ~0.1mm for the tube outer radius). The alternative code assumed a PERT distribution. The PERT distribution is a special case of the beta distribution and has the merit of giving zero probability outside a stated range (hence implementing drawing stipulated maximum and minimum values). Wall thicknesses are expected to reduce over life due to oxidation/corrosion effects on both the outer and inner surfaces (see §3).

2.3 Tube/Bifurcation Material

The bifurcations, the tailpipes and the boiler tubes at the top of the main boilers adjacent to the bifurcations are all composed of 316H austenitic stainless steel with compatible weld materials. Since they were not stress relieved after welding, the effects of residual stresses were included in the crack initiation assessment (see §5.2).

2.4 Assessment Locations and Stress Concentrations

Stresses are greatest on the inlet features to the bifurcation. Hence the chosen assessment locations were, as can be seen on Fig.1, (i)the weldment between the bifurcation inlet stub and the boiler tube, (ii)the radius feature at the section change on the bifurcation inlet stub, and, (iii)the root radius between the fins of the finned boiler tube at the tube-strap support nearest the bifurcation. Note that these are all local stress concentrations. Finite element analyses provided the stress concentration factors (SCFs) applicable to the axial stress for the parent radius features. For assessment location (ii) the SCF used was 1.97 or 2.12. For location (iii) the SCF was between 1.84 and 1.98. The range of SCFs reflects differences between loads (pressure versus bending) and also differences between the two codes used. The hoop stress was not subject to an SCF.

For assessment location (i), the weldment, an SCF of 1.14 was applied to account for the weld cap effect. However, for this location, the R5 creep-fatigue crack initiation procedure also requires the application of a “Weld Strain Enhancement Factor” (WSEF), which is a factor applied to the elastic-plastic strain rather than to the stress. The WSEF is defined against weldment type within the R5 procedure for weldments, and was taken to be 1.16. This value is specific to full-penetration butt welds. It is derived from data on the conventional fatigue strength reduction factor (FSRF) by splitting the latter into a part which increases the local stress and results from the weldment geometry (the WSEF) and a part which reduces the fatigue endurance due to the local material effects (the Weld Endurance Reduction, WER, see §5.2).

3. Temperatures, Flow Restrictions, Metal Losses and Chemical Cleans

3.1 Temperatures for Unrestricted Tubes

Temperature is, of course, a key input to any assessment involving creep. The three assessment locations are sufficiently close that their temperatures may be taken to be

the same. There are no direct measurements of metal temperatures in the vicinity of the bifurcations. Instead, the metal temperature is calculated from the temperatures of the fluids on either side. Denoting the steam temperature inside the tubes as T_{steam} and the reactor coolant carbon-dioxide temperature outside the tubes as T_{gas}, the metal temperature is found from,

$$T_{metal} = xT_{steam} + (1-x)T_{gas} \quad (1)$$

The dimensionless interpolation parameter, x, is found from the relative magnitudes of the heat transfer coefficients on the inner and outer surfaces. Actually there are no direct measurements of the fluid temperatures T_{steam} and T_{gas} at the bifurcation level either, though steam and gas temperature measurements are available at other heights in the boiler (including at the inlet and outlet). Consequently, the fluid temperatures at the bifurcation level are obtained from boiler models constrained by the available measurements at other heights. These boiler models are used routinely as part of the operational monitoring arrangements for the AGRs.

The models provide temperatures for each row of each pod of each reactor. Temperatures have varied over life, so model results have been obtained for a number of different time points (using linear interpolation between time points). The interpolation parameter, x, depends upon the fluid flow rates. The steam flow rate in a given tube depends upon the ferrule diameter at the boiler inlet. Different ferrule sizes are used for different rows as an attempt to minimise the "boiler tilt", i.e., the spread of outlet steam temperatures across the boiler. Consequently, the parameter, x, is also row-specific and has varied over life due to re-ferruling operations. Putting all these ingredients together in equation (1) provides a row-pod-reactor specific, time dependent, estimate of metal temperature. This is implemented in the probabilistic code via tabulated data for fluid temperatures and ferrule diameters at various times.

Uncertainty in the metal temperature is expressed via uncertainties in x, T_{steam} and T_{gas}. These variables were assumed normally distributed with standard deviations of 0.05, 8.377^{o}C and 10^{o}C respectively. The prescription for finding x is given in §3.2.

The probabilistic code uses these tube-specific, time varying, distributed temperatures. However, as an indication of the typical temperature of unrestricted tubes, Fig.2 shows the mean effective creep temperature (MECT) for each row (averaged over pods) of one reactor over the first 15 years of operation. The MECT is defined as that temperature which, if constant, would produce the same creep rupture damage as the actual temperature history. Fig.2 shows the substantial temperature difference between rows in early operation (subsequently ameliorated by re-ferruling).

3.2 Flow Restrictions and Corresponding Temperatures

In operation, corrosion products build up on the bore of the boiler tubes. For most tubes the effect on steam flow, and hence temperature, is minor. However, for a proportion of the inventory of tubes, the flow may become partly restricted, probably due to spalling of magnetite corrosion product in the ferritic regions of the boiler. In the reactor modelled here 398 tubes (~17% of the reactor inventory) have experienced flow restrictions at some time, though not all at the same time and many of these restrictions are very minor. However, the most severe restrictions of a few tubes can result in temperatures over a limited period approaching ~580^{o}C, considerably higher than for unrestricted tubes (Fig.2). An example of the temperature of a particularly severely restricted tube is shown in Fig.3 plotted against time. Each trial of the

probabilistic code will sample a different temperature-time curve, Fig.3 being the average of these samples for this specific tube. Future temperatures are based on the last flow measurement and fluid temperatures derived from recent operation, as illustrated by Fig.3.

Flow restrictions are periodically measured off-load. The flow resistance, K , is defined as the constant relating boiler pressure drop, ΔP (bar), to steam mass flow rate, $\dot{m}$ (kg.s^{-1}), and density, ρ (kg.m^{-3}), via,

$$\Delta P = K \frac{\dot{m}^2}{\rho} \tag{2}$$

so that K is in units bar s^2 kg^{-1} m^{-3}. A partially restricted tube is characterised by the excess of its flow resistance above the average for unrestricted tubes, $\Delta K = K - K_{unrestrcited}$. The probabilistic code includes tabulated data for ΔK for all tubes (essentially zero for unrestricted tubes) at a number of times. At intermediate times the larger ΔK of the last and the next measured time point is used. (The beneficial effect of chemical cleans, §3.4, in reducing ΔK is not claimed until confirmed by flow measurement).

The effect of flow restrictions is to reduce the steam-side heat transfer coefficient and hence to reduce the interpolation parameter x in equation (1), resulting in an increased metal temperature and a deleterious effect on creep life. This is taken into account in the probabilistic code via the following formulation for the interpolation parameter, x ,

$$x = \frac{x_0}{1 + ay + by \times MIN(y, c)} \tag{3}$$

where $y = 10^{-6} \Delta K$ (s^2 kg^{-1} m^{-3}). The parameters a, b, c and x_0 depend upon ferrule size but indicative values in units compatible with y are 3.403, -0.047, 1.5 and 0.818 respectively (giving outer surface metal temperature).

3.3 Metal Losses and Chemical Cleans

Metal losses occur over life due to steam side oxidation and CO_2 gas-side oxidation. In addition, intergranular attack (IGA) on the bore during off-load periods can lead to small losses of effective metal. The steam-side oxidation losses due to consecutive periods, t_i (khrs), at differing absolute operating temperatures, $\tilde{T}_i$ (K), but assuming no chemical cleaning operations, are calculated using,

$$\text{Steam-Side Oxidation Metal Loss} = 9.487 \times 10^6 \sqrt{\sum_i t_i \cdot 10^{\left(k - \frac{15{,}766}{\tilde{T}_i}\right)}} \tag{4}$$

The parameter k quantifies the oxidation reaction kinetics and was taken as normally distributed with a mean of 7.081 and a standard deviation of 0.133, the metal loss from (4) being in microns.

For the IGA metal losses, a log-normal distribution with a median value of 0.385 μm/khr was used, with a coefficient of variation (CoV) of 45%. However, regions affected by IGA will be removed by oxidation losses. Consequently the IGA loss is not simply additive to the steam-side oxidation loss. A time-dependent algorithm was

employed in which only the depth of IGA beneath the current oxidation/metal boundary was counted.

A conservative estimate of the CO_2 gas-side metal loss is given as a function of temperature, T (^oC), by,

For $t < 88khrs$: loss rate = 0.898 microns/khr (5a)

For $88khrs < t < 193khrs$: loss rate = 0.248 + 0.00587(T – 522^{o}C) microns/khr (5b)

For $193khrs < t$: loss rate = 0.205 + 0.00233(T – 522^{o}C) microns/khr (5c)

Uncertainty is expressed by multiplying (5a-c) by a log-normally distributed factor with a median of 0.633 and a CoV of 45.2%.

The boilers are subject to gradually increasing pressure drops over life due to the build up of corrosion products on the bore. These pressure drops are undesirable, leading to a greater potential for boiler instability. Consequently, chemical cleaning of the inside of the tubes has been carried out, three times for the reactor modelled. As well as reducing the boiler pressure drop such cleaning can be beneficial in reducing flow restrictions (though not invariably for all tubes). However chemical cleaning can lead to an increased rate of metal loss from the bore. This is due partly to the direct effect of the cleaning operation but mostly arises from the removal of oxide leaving bare metal exposed during the next period of operation, thus enhancing oxidation rates. The direct effect is to cause IGA, the mean depths of this IGA being $57\mu m$, $30\mu m$ and $30\mu m$ for the 1st, 2nd and 3rd chemical cleans respectively. These estimates were based on measured IGA depths following trials of the chemical cleaning process. Analyses of these data suggest a coefficient of variation of 45% and this was assumed in the probabilistic code.

The additional effect of chemical cleaning is to remove the oxide and this effectively resets the time datum in equation (4) to zero. Hence a sequence of consecutive periods at differing absolute operating temperatures $\tilde{T}_i$ (K) and of duration t_i (khrs) which are each separated by a chemical clean gives a total metal loss due to oxidation (in microns) of,

$$\text{Chemical Clean Adjusted Metal Loss} = 9.487 \times 10^6 \sum_i \sqrt{t_i} \cdot 10^{0.5\left(k - \frac{15{,}766}{\tilde{T}_i}\right)} \qquad (6)$$

Note that the metal losses depend upon several different distributed parameters, including the randomly sampled operating temperature. The temperature dependence means that there is an interaction between flow restrictions and metal loss rates.

Because the boiler tubes/bifurcation inlets are so thin, these metal losses can be a large proportion of the initial thicknesses. An illustration of the calculated variation of thickness over life is provided by Fig.4 for the bounding restricted tube. Hence the stresses can increase substantially over life, even if the loads were constant. Since creep is sensitive to stress, metal loss is a significant factor in the assessment.

4. Cycles, Loads and Stresses

The creep rupture assessments depend only upon the steady operating loads. However the assessment of creep-fatigue crack initiation to R5, Ref.[2], depends also upon the transient loads and the number and type of load cycles.

4.1 Cycle Types, Numbers and Sequence

The significant load cycles consist of start-up and shut-down (trip). The three major cycle types are, (i)reactor cycles to cold shutdown, (ii)reactor cycles to hot standby, and, (iii)cycles involving the isolation, and/or reinstatement, of a single boiler on a running reactor. It is important to distinguish between these three types of cycle because they correspond to different loadings. The historic sequence of these cycle types is known, together with their times of occurrence (in terms of operating hours). Consequently the actual sequence of cycles and associated operating periods (dwell times) was used in the assessment. The prediction of future cycle rates was based upon extrapolation from past rates, biasing the prediction towards recent years (operation in the earlier years being less indicative). This is intrinsically uncertain, of course. Nevertheless, the past and future patterns of cycling were treated as deterministic in the assessment.

A total of 223 reactor cycles plus 38 boiler cycles were assumed over a projected 40 year life of the reactor assessed. To-date, reactor cycles to cold shutdown and reactor cycles to hot standby conditions have been comparably frequent, but it is expected that cold shutdown cycles will be more frequent than hot standby cycles in future and this was reflected in the assessments. The creep dwell duration for each cycle is shown in Fig.5. The future dwells were derived from projected operating hours at salient times divided by the assessed number of cycles, i.e., the average length dwell of ~1500 hours was assumed for all cycles (Fig.5).

4.2 Pressures and Pressure Stresses

The bifurcations are subject to internal steam pressure and external carbon-dioxide coolant pressure. The steady operating pressures have varied a little over time, but for simplicity a single average value was assumed: 157.6 barg (steam) and 39 barg (CO_2) and hence a differential pressure of $\Delta P = 118.6$ barg. During reactor trips the steam pressure rises briefly. A bounding value for this transient steam pressure of 181.6 barg was used (a peak differential pressure of $\Delta P = 142.6$ barg).

The differential pressure in cold shutdown is zero. Boilers which have been powered-down and disconnected from a running reactor are either depressurised or nearly so. Hence the minimum pressure differential for boiler cycles is $\Delta P = -39$ barg (due to external pressurisation by the CO_2). The minimum steam pressure during hot standby conditions is more variable. Plant data was modelled by sampling the differential pressure ΔP from a distribution with mean 60.5 barg and standard deviation 16.5 barg, but, if this produced a result less than 43 barg replacing it with $\Delta P = -39$ barg. The fact that the minimum differential pressure in hot standby conditions can remain fairly high in some cases is significant in reducing the severity of these cycles (because the stress range is reduced compared with cycles to cold shutdown).

Elastic pressure stresses in the axial and hoop directions on the outer surface are given by,

$$\sigma_{axial}^{P} = SCF \times \frac{R_i^2}{R_o^2 - R_i^2}\Delta P \qquad \text{and} \qquad \sigma_{hoop}^{P,OD} = \frac{2R_i^2}{R_o^2 - R_i^2}\Delta P \tag{7}$$

where R_i, R_o are the randomly sampled inner and outer radii, including the time-dependent allowance for metal losses, and the SCF appropriate for the assessment location is used (see §2.4).

4.3 Steady Operating System Moments and Stresses

Substantial system loads arise in service due both to deadweight and to relative thermal expansions of the ferritic and austenitic parts of the boiler surface and support structures. The tailpipes attached to the bifurcations have a range of geometries. This leads to a wide range of system loads acting on different bifurcations. A number of tailpipe geometries were subject to finite element analysis to determine the system loads.

The deadweight loads (specifically the bending moments) were found to correlate with the 'overhang', i.e., the distance between the bifurcation and the first tube-strap support of the finned boiler tube (see Fig.1). This correlation was exploited to provide a best estimate of the deadweight system moments for every individual bifurcation in terms of the known overhangs. For assessment locations (i) and (ii) the best estimate deadweight bending moments (in Nm assuming the overhang in m) are given by,

Dual bifurcations: $$\overline{M}^{DW} = 14.15 \times overhang + 4.2 \quad (8a)$$

Mono bifurcations: $$\overline{M}^{DW} = 32.7 \times overhang + 1.6 \quad (8b)$$

For assessment location (iii) the corresponding results are,

Dual bifurcations: $$\overline{M}^{DW} = 7.2 \times overhang + 3.35 \quad (9a)$$

Mono bifurcations: $$\overline{M}^{DW} = 11.3 \times overhang + 5.7 \quad (9b)$$

The specific overhang for each tube is used in the probabilistic code. Fig.6 shows how the overhang is distributed across the inventory of bifurcations. Note that (8a,b,9a,b) show that, for a given overhang, the mono bifurcations are significantly more highly stressed than the dual bifurcations.

The error in deadweight moment was estimated by considering the scatter in the finite element model results for different tailpipe geometries about the trend line given by (8a,b,9a,b). The error was accounted for by a normally distributed multiplicative factor with a mean of unity and standard deviation 0.25 applied to (8a,b,9a,b). The same randomly sampled error variable is used for all three assessment locations (i.e., perfect correlation was assumed) on the physical grounds that high deadweight loading at one location is likely to imply high deadweight loading at the other locations due to their proximity. Different versions of the probabilistic code employed variants on this formulation, including assuming no correlation between the bifurcation and tube strap locations.

Thermal system loads were found from the finite element models at two different bifurcation temperatures, T_{un} = 522.4°C and T_{rest} = 578.9°C. These were used to provide a best estimate of the thermal bending moment (Nm) as a linear function of temperature. For assessment locations (i) and (ii),

Dual bifurcations: $$\overline{M}_{el}^{th}(T) = MAX\left[23.3, 23.3 + 11.2\left(\frac{T - T_{un}}{T_{rest} - T_{un}}\right)\right] \quad (10a)$$

Mono bifurcations: $$\overline{M}_{el}^{th}(T) = MAX\left[36.2, 36.2 + 11.2\left(\frac{T - T_{un}}{T_{rest} - T_{un}}\right)\right] \quad (10b)$$

For assessment location (iii),

Dual bifurcations: $$\overline{M}_{el}^{th}(T) = MAX\left[15.7, 15.7 + 17.7\left(\frac{T - T_{un}}{T_{rest} - T_{un}}\right)\right] \quad (11a)$$

Mono bifurcations: $$\overline{M}_{th}^{el}(T) = MAX\left[31.5, 31.5 + 12.0\left(\frac{T - T_{un}}{T_{rest} - T_{un}}\right)\right] \quad (11b)$$

The thermal moments are randomly sampled from a normal distribution with mean given by (10a,b) or (11a,b) and with a standard deviation of 10.0 Nm for (10a,b), 5.3 Nm for (11a) and 13.8 Nm for (11b). If the sampled value for M_{el}^{th} is negative then it is replaced by $\left|M_{el}^{th}\right|$ for conservatism. Different versions of the probabilistic code employed variants on this formulation, including truncating negative values to zero. Separately sampled error variables were used for the thermal moments at the bifurcations (locations (i) and (ii)) and at the tube strap (location (iii)), i.e., assuming no correlation, based on the finite element evidence.

Bending moments are converted to elastic bending stresses at the outer fibre using,

$$\sigma_{axial,gb}^{sys} = SCF \times \frac{MR_o}{I}, \text{ where, } I = \frac{\pi}{4}\left(R_o^4 - R_i^4\right) \text{ and } M = M^{DW} + M^{th} \quad (12)$$

(In general the thermal moment, M^{th}, may differ from its elastic values, M_{el}^{th}, due to relaxation, see §5).

Including the pressure stress, the total axial stress is $\sigma_{axial}^{tot} = \sigma_{axial}^{P} + \sigma_{axial,gb}^{sys}$ and the elastic Mises stress on the outer fibre is thus,

$$\overline{\sigma}_{el}^{OD} = \left[\left(\sigma_{axial}^{tot} - \sigma_{hoop}^{P,OD}\right)^2 + \left(\sigma_{axial}^{tot} + P_{gas}\right)^2 + \left(\sigma_{hoop}^{P,OD} + P_{gas}\right)^2\right]^{1/2} / \sqrt{2} \quad (13)$$

For the purposes of the R5, Ref.[2], creep-fatigue crack initiation assessment an equivalent stress range is required, defined like (13) in terms of the component ranges, thus,

$$\Delta\overline{\sigma}_{el}^{OD} = \left[\left(\Delta\sigma_{axial}^{tot} - \Delta\sigma_{hoop}^{P,OD}\right)^2 + \left(\Delta\sigma_{axial}^{tot} + \Delta P_{gas}\right)^2 + \left(\Delta\sigma_{hoop}^{P,OD} + \Delta P_{gas}\right)^2\right]^{1/2} / \sqrt{2} \quad (14)$$

4.4 Transient System Moments and Cycle Dependent Sampled Variables

Even for a given cycle type, every cycle will in general be different. A number of distributed variables were used to model these cycle-to-cycle differences. These included, (i)the transient peak in the thermal stress which occurs during start-up, (ii)the transient peak in thermal stress which occurs during reactor trip, and, (iii)the minimum temperature reached during a hot standby condition. These factors can have a major bearing on the outcome of an assessment. For example, a large start-up stress tends to suppress the dwell stress and hence to reduce the assessed creep damage. If the temperature during a hot standby remains high then the associated thermal stress range with respect to the operating condition will be much smaller than would apply for a cold shutdown. This makes the corresponding cycle less severe. Indeed, if the cycle is elastic as a consequence, it may also make the following creep dwell far less onerous (see §5.2). Alternative versions of the probabilistic code accounted for these cycle-dependent variables in different ways. One approach is illustrated below.

Fig.7 plots the peak thermal stresses during reactor start-ups in the form of factors over the steady operating thermal stress. These data were obtained by examining the temperatures around the boilers during a range of plant start ups. The probabilistic

code randomly samples the distributions of Fig.7 for each reactor cycle. Note that the inner rows (1 to 6) have substantially smaller thermal transient factors than the outer rows and that this will result in the inner rows having larger assessed creep damage, other things being equal. Fig.8 shows the equivalent transient thermal stress factors for reactor trips. Fig.8 does not conform to any standard probability density function, consisting of two separate populations. This illustrates why it can be best to sample the distribution of plant data directly, as was done in this case.

Fig.9 shows the histogram of minimum temperatures, $T_{\min}$, during hot standby conditions. This histogram is sampled for each reactor cycle to hot standby conditions. Examination of a few cases suggested that a reasonable estimate of the minimum thermal stresses would be given by factoring the steady operating thermal stresses by $\sqrt{(T_{\min} - 20)/(T - 20)}$ where T (^{o}C) is the normal operating temperature.

Transient data were also coded in a similar manner for boiler trips and boiler reconnection cycles.

5. Deterministic Assessment Methodology

A Monte Carlo probabilistic assessment consists of carrying out a large number of deterministic assessments with different, randomly sampled, values of the distributed parameters. Hence, the core of the probabilistic code is deterministic assessment to R5, Ref.[2]. This deterministic core is described in this section.

5.1 Creep Rupture

Time to rupture is assessed, following the R5, Ref.[2], procedure, by entering a rupture reference stress into a suitable empirical rupture equation for 316H material. The rupture reference stress is defined by,

$$\sigma_{ref}^{R} = \left[1 + 0.13(\chi - 1)\right]\sigma_{ref} \qquad \text{where, } \chi = \frac{\bar{\sigma}_{el}^{\max}}{\sigma_{ref}} \tag{15}$$

where σ_{ref} is a reference stress and $\bar{\sigma}_{el}^{\max}$ is the peak elastic Mises stress, eq.(13). A suitable combined load reference stress solution was taken to be,

$$\sigma_{ref} = MAX\left[\frac{\Delta P}{\ln\left(\frac{R_o}{R_i}\right)}, \sqrt{\frac{3}{4}\left(\frac{\Delta P}{\ln\left(\frac{R_o}{R_i}\right)}\right)^2 + \left(\frac{3}{4}\cdot\frac{M}{\left(R_O^3 - R_I^3\right)}\right)^2}\right] \tag{16}$$

where M, R_I, R_O are all time-varying, the latter being the inner and outer radii. ΔP is the differential pressure across the tube and M is the deadweight plus thermal moment under steady full power operation. This reference stress solution is in common use for power plant pipework assessments. When the bending moment is small it reduces to the exact Tresca limit load solution for a thick walled pipe under internal pressure assuming an elastic-perfectly plastic material (as derived in standard structural mechanics texts, e.g. Ref.[20]). A significant bending moment is accommodated via assumed circular interaction between the corresponding Mises solution for pressure and the usual lower bound solution for bending. This reference stress solution assumes that the system axial force is small, a fact confirmed by the

finite element models. The time to rupture, $t_{rup}\left(\sigma_{ref}^{R},T\right)$, is thus found for the currently prevailing rupture reference stress and temperature, T . The pressure and deadweight loads are assumed primary, but the thermal load is assumed secondary with some elastic follow-up factor, Z . The rupture reference stress as defined above, calculated from the combined loads, will therefore be subject to relaxation by creep. This can be determined by integration of,

$$\frac{d\sigma_{ref}^{R}}{dt}=-\frac{\overline{E}}{Z}\left[\dot{\varepsilon}_{c}\left(\sigma_{ref}^{R},\varepsilon_{c},T\right)-\dot{\varepsilon}_{c}\left(\sigma_{\mathrm{Pr}}^{R},\varepsilon_{c},T\right)\right] \tag{17}$$

where $\dot{\varepsilon}_{c}\left(\sigma,\varepsilon_{c},T\right)$ is the creep strain rate at stress σ and temperature T for an accumulated creep strain of ε_{c} (strain hardening being assumed), and σ_{Pr}^{R} is the rupture reference stress based on primary loads alone (i.e., pressure and deadweight only). The first term on the right-hand side of eq.(17) would be the relaxation rate if the initial stress were entirely secondary, with elastic follow-up factor Z. However, the stress cannot relax below the primary stress. This is ensured by the second term in eq.(17) which causes the curve of stress against time to become asymptotic to the primary rupture reference stress, σ_{Pr}^{R}, if the creep dwell is sufficiently long. More generally it reduces the rate of relaxation and this results in a larger accumulated creep strain in the dwell, $\Delta\varepsilon_{c}$, than would have been the case if the second term were omitted.

Integration of the relaxation equation was carried out numerically using finite time steps. For each time increment in the integration of eq.(17), and hence for each relaxed stress σ_{ref}^{R}, the rupture time, $t_{rup}\left(\sigma_{ref}^{R},T\right)$, is re-calculated. The creep rupture damage is defined via the time fraction, i.e., by the summation of $\Delta t/t_{rup}$ over every time increment, Δt . Note that the effect of metal losses and temperature variations over life means that σ_{ref}^{R} does not necessarily decrease monotonically. Increases of temperature (e.g., due to the occurrence of a flow restriction) will increase the thermal moment, whilst thickness loss will tend to increase all stresses. Hence the 'relaxing' σ_{ref}^{R} must periodically be adjusted to take account of these effects and may increase in some periods.

In the probabilistic code, the rupture damage will depend upon the random sampling inherent in a host of variables, including the loads, the initial dimensions, the metal losses, the flow restrictions, the operating temperatures – and, of course, the scatter in the creep rupture data.

5.2 Creep-Fatigue Crack Initiation

The creep-fatigue crack initiation methodology follows R5 Volume 2/3, Ref.[2], but including some refinements which are anticipated for weldments. The basic idea of the R5 Volume 2/3 approach is, for each of the three assessment locations,

[1] For a given plant cycle, construct the stress-strain hysteresis cycle, which for the present application is generically like Fig.10;

[2] Use the strain range derived from this hysteresis cycle construction to calculate the fatigue endurance and hence the fatigue damage due to this cycle;

[3] Use the start-of-dwell stress derived from this hysteresis cycle construction to calculate the creep relaxation and hence the creep damage due to this cycle;

[4] Repeat the above procedure for all cycles, past and future, to evaluate the cumulative damage (defined as the sum of the creep and fatigue damages).

[5] Crack initiation is conceded if damage reaches unity at any one of the three assessment locations.

A very brief description of each of the assessment steps [1-3] is presented below, though necessarily not the full details (for which see Ref.[2]).

Hysteresis Cycle Construction

The R5 procedure uses the elastic stresses, converted to Mises stress ranges. Referring to Fig.2 we shall interpret the salient points on the cycle, for illustrative purposes, as,

A = cold shutdown;
C = peak of transient start-up stress;
D = start of steady, full power operation
E = end of period of steady operation, just prior to trip
G = peak of transient stress during trip;
J = hot standby condition

The part cycle ABC is constructed by converting the elastic Mises stress range between points A and C to an elastic-plastic stress and strain range using the Neuber construction. The Neuber construction consists of the assumption that the product of the stress and strain ranges remains invariant as yielding proceeds, together with the requirement that the stress and strain ranges fall on the required cyclic stress-strain curve (given, in this case, by a Ramberg-Osgood equation). The absolute positioning of ABC along the stress axis can be fixed by "symmetrisation". This is defined in R5, Ref.[2], as the requirement that each end of the cycle protrude equally beyond the value of $K_S S_y$ evaluated at the corresponding temperature. Here S_y is the 0.2% proof stress and K_S is an empirically based, and temperature dependent, shakedown factor. (In a deterministic R5 assessment, S_y is defined as the lower bound 0.2% proof stress, but for our probabilistic assessment it is re-defined as the sampled value of the 0.2% proof stress for the current trial). A variant on the "symmetrisation" method of positioning the cycle, which took into account cycle interaction, was also explored but found to make little difference to the probability of crack initiation.

Points G and J on Fig.10 are found in a similar manner, using the elastic Mises stress ranges A-to-G and G-to-J respectively. R5 also advises variants on the type of Ramberg-Osgood equation to employ for different part cycles, see Ref.[2].

For the weldment location the procedure is modified by factoring the elastic-plastic strain ranges by the WSEF (see §2.4) and finding stress ranges so as to be compatible therewith.

Fatigue Damage

The elastic-plastic strain ranges calculated as described above for the half-cycles A-to-G and G-to-J are enhanced by a volumetric correction, and also, for the former, by the increment of creep strain in the dwell. The larger of the two resulting strain range estimates is used to calculate the fatigue damage. R5, Ref.[2], requires that laboratory fatigue endurance data be adjusted for the depth of crack assumed to constitute 'initiation'. This has been taken as 0.2mm, which leads to a reduction in the assumed endurance. In the case of weldments there is a further reduction by the WER (§2.4) which consists of ignoring the incubation phase (corresponding to the production of a

microcrack of depth 0.02 mm). This is simply a surrogate for specific weldment fatigue endurance data.

Creep Damage

In contrast to creep rupture, for which creep damage is defined via the time fraction, the creep damage in an R5 Volume 2/3 creep-fatigue crack initiation assessment is defined via ductility exhaustion, i.e., as a strain fraction. The start-of-dwell stress, σ_D, is found by elastically unloading from the stress at C by the amount by which the start-up peak stress exceeds the steady full power stress. The relaxation from D to E is found by integrating eq.(17) but with σ_{ref}^R replaced by a stress which starts at σ_D. However, if this is less than the rupture reference stress *based on primary loads only*, σ_{Pr}^R, then this primary rupture reference stress, σ_{Pr}^R, is used as the dwell stress, which therefore does not relax.

An issue of crucial importance to the outcome of the assessment is whether the creep strain accumulated during a dwell is carried over to the next cycle, hence causing continuous hardening and reducing creep strain increments cycle-on-cycle (other things being equal). The alternative assumption is that primary creep starts at datum time zero on every cycle, referred to as "primary reset". This leads to faster creep strain rates and hence larger creep damage. To discriminate between continuous hardening and primary reset, data from a number of creep-fatigue tests on 316H material at 550^{o}C were examined. These implied that, whilst primary reset was conservative it matched the test relaxations far better than continuous hardening which appeared to be insupportable. An example for just one such test, which used one hour dwells at 550^{o}C, is shown as Fig.11. This plots the start of dwell stress and the end of dwell stress obtained from the test against accumulated creep hours (which is the same as the number of cycles in this case). Fig.11 shows the initial cyclic hardening followed later by cyclic softening, though it is the relaxation in the creep dwell which is of interest here. The forward creep rate of the cast of material used in the test was determined and this forward strain rate used to calculate the expected relaxation using an equation like (17). The end of dwell stress calculated on the basis of continuous hardening, and also on the basis of primary reset, is shown in comparison with the test data on Fig.11. The use of continuous hardening under-estimates the relaxation and hence would under-estimate the creep damage based on ductility exhaustion. The use of primary reset, in contrast, over-estimates the relaxation.

A distributed parameter, ζ, was defined which adjusted predictions based on primary reset to match the test data (on Fig.11 this corresponds to re-scaling the green curve to the dashed curve). This formed the basis of the assessment procedure applied to the bifurcations. However this procedure was deemed relevant only when reverse plasticity had occurred between one creep dwell and the next. In effect the reverse plasticity is assumed to be responsible for the resetting of primary creep. Consequently if unloading (i.e., G-to-J in Fig.2) occurs elastically, then the subsequent creep dwell was calculated assuming continuous hardening, as if the creep process had not been interrupted. The criterion adopted for being effectively elastic was a reverse plastic strain of less than 0.01%.

Finally, the total creep strain increment for a given cycle ($\Delta\varepsilon_c$) was used to find the increment of creep damage, $\Delta D_c = \Delta\varepsilon_c / \bar{\varepsilon}_f$, where $\bar{\varepsilon}_f$ is the randomly sampled creep

ductility for the trial in question, including factoring for multiaxial effects as specified in R5, Ref.[2].

Treatment of Residual Stresses

In reality the early elastic-plastic hysteresis cycles are likely to have eradicated the welding residual stresses before they could cause significant creep damage. This is especially the case here since the first operational load cycles were below the creep regime. However, R5, Ref.[2], does require that an allowance for creep damage due to welding residual stress relaxation be included in the assessment.

The following crude algorithm was used. Initial hoop and axial residual stresses of 350 MPa and 280 MPa respectively were assumed. These are rather arbitrary except for being an overly conservative allowance (being far larger than the proof strength at operating temperature). The total elastic Mises stress at the start-up peak of the first cycle is evaluated by combining the residual stresses and the operational deadweight, pressure and thermal stresses. The Neuber construction is employed to convert this total elastic Mises stress to an elastic-plastic Mises stress. This stress is reduced by the elastic unloading between the start-up peak and normal operation (if applicable). The amount by which the stress derived in this way exceeds the start-of-dwell stress calculated for the first cycle ignoring residual stress is the extra stress due to the residual stress, σ_{res}. The additional creep damage due to residual stresses is estimated from $D_c^{res} = \frac{Z\sigma_{res}}{\bar{E}\bar{\varepsilon}_f}$.

6. Monte Carlo Probabilistic Simulation Methodology

The Monte Carlo method involves randomly sampling the distributed input variables many times, carrying out a deterministic assessment for every trial. Latin hypercube sampling was used, Ref.[3]. This is an efficient simulation technique which permits a large number of distributed variables to be addressed. Each variable can take one of a finite number of values each of which represents a range of values (a 'bin'). All bins are of equal probability. The Latin hypercube algorithm ensures that all bins of all variables are sampled in the minimum number of trials (though not, of course, in all possible combinations). Moreover, because all bins are of equal probability it follows that all trials are of equal probability, thus ensuring that all trials are of equal weight in the simulation.

The estimated probability that a crack initiates, or creep rupture occurs, in a given component is then simply the ratio of the number of trials which crack (or rupture) divided by the total number of trials for that component. Alternatively, for the simulation of a population of components, the frequency of cracks initiating, or failure by creep rupture occurring, is estimated by the ratio of the total number of crack initiations (or failures) in a given year divided by the total number of simulations, each of which covers the whole population of components.

Different codes were written for creep rupture and creep-fatigue crack initiation. In fact both versions were written twice, independently by each of the authors for the purposes of verification. The exact set of distributed variables differed slightly between versions but a typical set is listed below. The type of distribution used is indicated in brackets. As a general rule a lognormal distribution was used in preference to a normal distribution if the variable was positive definite and the coefficient of variation was large. Use of a lognormal distribution in such cases avoids

the problem of sampling impossible negative values which might arise if a normal distribution were used. The term “histogram” here refers to the use of plant data to define a histogram of values which was sampled directly rather than fitted to a standard probability density function.

- Start-of-life (sol) inner and outer radii for the bifurcation inlet stub and the finned tube (PERT, see §2.2);
- Overhang distribution (deterministic or histogram, Fig.6);
- Parameters representing metal losses from the inner surface due to oxidation, carburisation, inter-granular attack (IGA) and chemical cleaning (see §3.3);
- Metal loss from the outer surface due to CO_2 oxidation (lognormal, §3.3);
- Deadweight and thermal moments in steady full power operation at the bifurcation inlet and at the tube-strap position (normal, §4.3);
- The mean effective creep temperature (MECT) for unrestricted tubes (normal, §3.1);
- Gas temperature at the bifurcation location (normal, §3.2);
- Superheater outlet steam temperature (normal, §3.2);
- The parameter, x, used to interpolate the metal temperature from the fluid temperatures (normal, §3.2);
- The 0.2% proof stress, distinct for the bifurcation and tube materials (lognormal);
- The cyclic stress-strain Ramberg-Osgood equation A parameter, sampled separately for tube and bifurcation in some cases (lognormal);
- Young's modulus, sampled separately for tube and bifurcation in some cases (lognormal);
- The fatigue endurance, sampled separately for each of the three assessment locations in some cases (lognormal);
- The peak thermal stress during start-up and trip, distinct distributions (uniform or histogram, §4.4);
- The minimum temperature and minimum differential pressure during hot standby (uniform or histogram, §4.2 and §4.4);
- The creep strain rate, sampled separately for the three assessment locations in some cases (lognormal);
- The creep ductility, sampled separately for the three assessment locations in some cases (lognormal);
- The creep rupture life, sampled separately for the three assessment locations in some cases (lognormal);
- The relaxation correction factor, ζ (lognormal, §5.2);
- Elastic follow-up factor, Z (PERT or histogram).

Up to 41 distributed variables were used.

7. Input Correlations

The issue of correlations is crucial in a probabilistic assessment. This may involve, (i)correlations between material properties, (ii)correlations between a material property and stress or temperature, (iii)correlations between locations, or, (iv)correlations between loads. An example of an important correlation between material properties occurred in the rupture assessment in which the creep deformation (strain rate) and the creep rupture strength were taken to have a correlation coefficient of -0.80 to -0.73 (the negative value indicating that high rupture strength is associated with low creep strain rates). No correlations between material properties were

assumed in the crack initiation assessment. However, material properties commonly depend upon temperature and where relevant this temperature dependence was explicitly included in their formulation. The issue of a possible (negative) correlation between creep ductility and stress is problematic and hence, for simplicity and conservatism, no such correlation was assumed. An example of a correlation between locations is the use (in some cases) of just one error variable for the deadweight moment at several locations, this being equivalent to perfect correlation. In contrast, the thermal loads at these locations are uncorrelated, the error variable being sampled separately for each location. An example of an implicit correlation between loads is provided by the treatment of the transient thermal loads in start-up and trip. These were implemented as factors by which to multiply the steady operating thermal stress. Hence, if the steady operating thermal stress happens to be randomly sampled in some trial to have a large value, then the transient thermal stresses for all cycles of that trial will tend to have large values. This is conservative rather than necessarily strictly correct.

8. Implementation and Convergence

The probabilistic programs were implemented in Excel using Visual Basic for the bulk of the coding. One version of the code used the proprietary add-on RiskAMP, Ref.[21], to implement the Monte Carlo Latin hypercube sampling algorithm, but an alternative version, used for verification, coded the Latin hypercube algorithm independently in Visual Basic.

A trial is defined as the evaluation of the total damage over the projected 40 year life for all three assessment locations, for a single tube/bifurcation and for a single set of randomly sampled variables. In the case of crack initiation assessments, one trial therefore involves the construction of 261 different hysteresis cycles for each of the three assessment locations.

Sufficient numbers of random trials must be carried out to obtain converged results. To find reactor-averaged creep rupture probabilities, 20,000 trials were used for the inventory of restricted tubes (50 trials per tube) and ~23,400 trials for the inventory of unrestricted tubes (12.5 trials per tube). To find whole reactor crack initiation rates, 50,000 trials were used for the restricted tubes and 250,000 for the unrestricted tubes (about 130 trials per tube). Whilst this number of trials proved sufficient for whole reactor or reactor averaged quantities it was not sufficient to obtain converged results for individual tubes. In cases where probabilities were required for individual tubes, 4,500 trials per tube were used for rupture and 10,000 trials per tube were used for crack initiation.

On standard desktop PCs with a core i5-2400 processor (quad core), run times of 0.045 seconds per trial were achieved for creep rupture simulations and 0.15 seconds per trial for crack initiation. The task overall addressed around 22 million trials. This included many sensitivity studies as well as applying two independent codes for verification purposes.

Convergence was determined in two ways: by convergence of the failure/cracking probability in real time during the execution of the code, and by re-running the same input to confirm that an acceptably close result was obtained each time. As an example for creep rupture, five re-runs of 4,500 trials all produced results within 5% of their mean. Fig.12 provides an example of a convergence check for the crack initiation assessments, showing both how a single run converges in about half the

50,000 trials used in this example (for restricted tubes) and also how a repeat run converges to (almost) the same result.

9. Results

Results were obtained separately for creep rupture and creep-fatigue crack initiation. The results given are for one particular example reactor. The reactor in question has undergone three campaigns of whole-reactor chemical cleaning.

9.1 Results of the Creep Rupture Assessments

The annual creep rupture probability per tube, averaged over the next 12 years, is shown in histogram form in Fig.13 (restricted tubes) and Fig.14 (unrestricted tubes). Around half of the bifurcations have rupture probabilities in the order of 10^{-4} per year, though a small number of bifurcations have rupture probabilities an order of magnitude larger than this. This is true both for tubes with and without a restriction history. The rupture probability is not markedly greater for tubes with a restriction history, though a small difference can be resolved, as illustrated by Fig.15. This Figure shows how the annual rupture probability increases over life. Time-dependent failure mechanisms generally produce increasing failure rates of which Fig.15 is typical. Some salient results were,

- The average annual rate of tube failure by creep rupture over the remaining years of an assumed 40 year life is ~0.23 failures per reactor year (or about 3 future failures);
- The assumption that creep deformation and creep rupture are negatively correlated is crucial to this prediction, the number of failures predicted being a factor of ~7 times greater if no correlation is assumed;
- The annual rate of tube rupture is predicted to increase by a factor of about 3 or 4 over the next 12 years (though remaining at a low rate over this period);
- The deleterious effect of a whole-reactor chemical clean on the rupture probability as a result of additional metal loss is very slight;
- The rupture probability is dominated by the contribution from the unrestricted tubes, as a consequence of their numerical preponderance over tubes with a restriction history.

9.2 Results of Creep-Fatigue Crack Initiation Assessments

In trials which predicted crack initiation, the fatigue damage was always negligible, the prediction of cracking being strongly creep dominated.

Fig.16 illustrates the contribution that the assumed residual stresses make to the creep damage. It is very small and repeating runs with no residual stress confirms that the residual stresses have no discernable effect upon the probability of cracking.

Fig.17 plots the predicted number of cracks initiating over the whole reactor against operating hours (the right hand of the time axis, 265,000 hours, being 40 elapsed years). About 3 cracks are predicted by the end of life. Fig.17 shows that this prediction is dominated by the unrestricted tubes due to their numerical preponderance over the tubes with a restriction history. Fig.17 also shows that the annual rate of cracking is predicted to increase (by a factor of around 3 between now and the end of a 40 year life).

Fig.18 is the histogram over all trials of the percentage of dwells per trial for which the start-of-dwell stress is set equal to the rupture reference stress. Recall that this is done only if the hysteresis loop construction results in a smaller start-of-dwell stress. Fig.18 shows that the histogram over all trials is emphatically different from that which is confined to trials which predict cracking. Trials which do not crack typically use the rupture reference stress (i.e., the minimum possible start-of-dwell stress) for almost all cycles. In contrast, trials which predict cracking typically use the (larger) hysteresis-based start-of-dwell stress for about 50% of the cycles.

Fig.19 is a similar histogram of the percentage of dwells per trial which use primary creep reset, as opposed to continuous hardening, to calculate creep relaxation. Again there is an emphatic difference between the histogram over all trials and that confined to just trials which predict cracking. In the former the use of primary reset is rare. In the latter, however, typically half the cycles employ primary reset. The use of primary reset implies significant reverse plasticity. Hence the histograms of trials which initiate cracks in both Figs.18 and 19 may be attributed simply to the sampling of higher stresses. In other words these Figures identify the uncertainty in stress as being of particular significance in the prediction of cracking.

More generally those parameters which are of greatest significance in causing cracking can be identified by evaluating their correlations with the end of life damage. This was done systematically for a number of parameters. The four most significant factors and their typical correlation coefficients were,

Thermal system moment:	~0.31
Creep deformation rate:	~0.24
Creep ductility:	~0.16
Metal temperature:	~0.165 (restricted), ~0.124 (unrestricted)

This confirms the conclusion based on Figs.18,19 that the uncertainty in stress, specifically the thermal system stress, is particularly important in causing cracking. What the probabilistic simulation elucidates, which would not be apparent from a deterministic assessment, is that stress is twice as important as the operating temperature in causing cracking (as judged from the correlation coefficients). The creep deformation rate, which is highly scattered, is also one of the top determinants of cracking, whilst the creep ductility is also important but somewhat less so. The fact that none of the correlation coefficients exceeds ~0.31 demonstrates that the occurrence of cracking is multi-factorial: no one factor results in cracking but rather a number of parameters must attain onerous values to produce cracking. This, of course, is the reason why the probability of cracking per tube is small.

Like any other method, the probabilistic method is only as reliable as its inputs. Where there is major ambiguity in how a variable is to be quantified as a distribution, the method contains no ‘magic’ to compensate for this. An example in this application was in regard to the significance of the deadweight system moments. Differences in the manner of representing the finite element results for deadweight loading as probability distributions led to significant differences in the predicted importance of deadweight loading between the two versions of the code. In one case the correlation coefficient was found to be small (~0.05) whilst the alternative code resulted in cracking being quite strongly correlated with the overhang (in terms of which the deadweight loading is defined). However this was a rare exception to the general

rule that the two independent codes agreed well, despite many differences in the details of their implementation.

10. Discussion and Conclusions

Probabilistic assessment provides quantitative estimates of the rupture and crack initiation probabilities. An advantage of probabilistic assessments is that they also provide a balanced view of which factors are most significant. This tends to be obscured in traditional deterministic assessments as a consequence of deploying many bounding assumptions. In the application considered here an illustration of this is in respect of the significance of partial flow restrictions. Deterministic assessments have resulted in a considerable focus of attention on restricted tubes, whereas the probabilistic treatment reveals that restrictions are much less dominant in their structural effect. The numerical preponderance of unrestricted tubes means that they dominate the rupture and crack initiation probabilities, despite the occurrence of a flow restriction increasing the probabilities for individual tubes. This puts the threat posed by partial flow restrictions into perspective, provided it continues to be properly managed.

The factors that are most significant in determining rupture and crack initiation probabilities are the stresses, the material creep properties and their correlations and aspects of the assessment methodology (especially the primary creep reset issue in the crack initiation assessments). The importance of the stresses, and their uncertainties, highlights the desirability of quality pipework analyses to determine the system stresses in the boiler tubes, tailpipes and boiler surface features generally, noting that system stresses are often larger than the pressure stresses. It is sometimes falsely assumed that the flexibility of boiler tubing implies that the system stresses are small. But in truth their flexibility means only that the system *loads* are small, not the corresponding stresses.

Assessments are often based simply on creep rupture. However it is possible in principle that crack initiation followed by crack growth might provide a more rapid failure mechanism. This has been explicitly ruled out for the present application by the probabilistic assessments of both rupture and crack initiation. Given the unquantified but significant margin between crack initiation and leakage/failure, the fact that very few cracks are predicted to initiate by end of life implies that the initiation-then-growth mechanism is not limiting. For this application an adequate assessment would therefore be provided by considering creep rupture only, though this can be concluded only because the creep-fatigue crack initiation assessment has been carried out. The conclusion is valid, of course, only if no crack initiation mechanisms other than low cycle creep-fatigue are active.

The predicted rates of rupture/cracking by the creep-fatigue mechanism are tolerable and not expected to challenge commercial operation for a projected 40 year life. Both the annual rupture probability and the annual rate of crack initiation are predicted to increase by a factor of around 3 between now and the end of a 40 year operational life, indicative of accumulating creep damage. Consequently the creep-fatigue mechanism could potentially become a significant factor in managing plant lifetime beyond 40 years. The probabilistic assessment techniques reported here would provide a means of quantifying risk beyond that time.

11. References

[1] Holt P J, Bradford R A W. Application of probabilistic modelling to the lifetime management of nuclear boilers in the creep regime: Part 1. Int J Press Vess Piping 2012; 95:48-55.

[2] R5, "Assessment procedure for the high temperature response of structures", R5 Issue 3, June 2003, EDF Energy. (See also D.W.Dean, P.J.Budden and R.A.Ainsworth, "R5 procedures for assessing the high temperature response of structures: current status and future developments", In: Proceedings of PVP2007, the 2007 ASME pressure vessels and piping division conference. San Antonio, Texas, USA; July 22e26 2007, paper PVP2007-26569).

[3] Kroese D P, Taimre T, Botev Z I. Handbook of Monte Carlo methods, Wiley series in probability and statistics. Wiley-Blackwell; April 2011.

[4] Yatomi M, Nikbin K M. Sensitivity analysis of creep crack growth prediction using the statistical distribution of uniaxial data. Fatigue Fract Eng Mater Struct September 2010;33:549-61.

[5] Nikbin K M, Yatomi M,Wasmer K,Webster G A. Probabilistic analysis of creep crack initiation and growth in pipe components. Int J Press Vess Piping July-August 2003;80:585-95.

[6] Kim W G, Park J Y, Hong S D, Kim S J. Probabilistic assessment of creep crack growth rate for Gr.91 steel. Nucl Eng Des Sept.2011;241:3580-6.

[7] Wei Z, Yang F, Lin B, Luo L, Konson D, Nikbin K. Deterministic and probabilistic creep–fatigue–oxidation crack growth modelling. Probabilistic Engineering Mechanics July 2013;33:126–134.

[8] Wei Z, Yang F, Cheng H, Nikbin K. Probabilistic Prediction of Crack Growth Based on Creep/Fatigue Damage Accumulation Mechanism. Journal of ASTM International May 2011;8:103690.

[9] Roy N, Ghosh R N, Bose S C. A Stochastic Model for Evolution of Creep Damage in Engineering Material. 5th International Conference on Creep, Fatigue and Creep-Fatigue Interaction September 24-26, 2008, Kalpakkam, India.

[10] Kim W-G, Park J-Y, Kim S-J, Jang J. Reliability assessment of creep rupture life for Gr. 91 steel. Materials & Design Oct.2013;51:1045–1051.

[11] Rahman S, Ghadiali N, Wilkowski GM, Paul D. A computer model for probabilistic leak-rate analysis of nuclear piping and piping welds. Int J Press Vess Piping March 1997;70:209-21.

[12] Rajasankar J, Iyer N R, Appa Rao T V S R. Structural integrity assessment of offshore tubular joints based on reliability analysis. Int J Fatigue July 2003;25: 609-19.

[13] Delph T J, Berger D L, Harlow D G, Ozturk M. A probabilistic life prediction technique for piping under creep conditions. J Press Vess Tech Oct.2010;132: 051206.

[14] Zhao J, Li D M, Zhang J S, Feng W, Fang Y Y. Introduction of SCRI model for creep rupture life assessment. Int J Press Vess Piping Sept.2009;86:599-603.

[15] Deschanels H, Escaravage C, Le Mat Hamata N, Colantoni D. Assessment of industrial components in high temperature plant using the ALIAS-HIDA e A case study. Eng Fail Anal July 2006;13:767-79.

[16] Zhou C, Tu S. A stochastic computation model for the creep damage of furnace tube. Int J Press Vess Piping Sept.2001;78:617-25.

[17] Penny R K, Weber M A. Robust methods of life assessment during creep. Int J Press Vess Piping 1992;50:109-31.

[18] Hu D and Wang R. Probabilistic Analysis on Turbine Disk Under LCF-Creep, ASME conference turbo expo 2008: power for land, sea and air (GT2008), vol. 5. Berlin: Structures and Dynamics; June 9-13.

[19] Huang J L, Zhou K Y, Xu J Q, Xu X H. Probabilistic creep rupture life evaluation of T91 alloy boiler superheater tubes influenced by steam-side oxidation. Materials & Corrosion, published online May 2013, DOI: 10.1002/maco.201206963.

[20] Benham P P, Crawford R J, Armstrong C G. Mechanics of Engineering Materials. Pearson / Prentice Hall, 2nd ed 1996.

[21] RiskAMP Monte Carlo Add-In for Excel, Structured Data LLC, New York.

Fig.1. Photograph of superheater bifurcations in-situ in a boiler pod

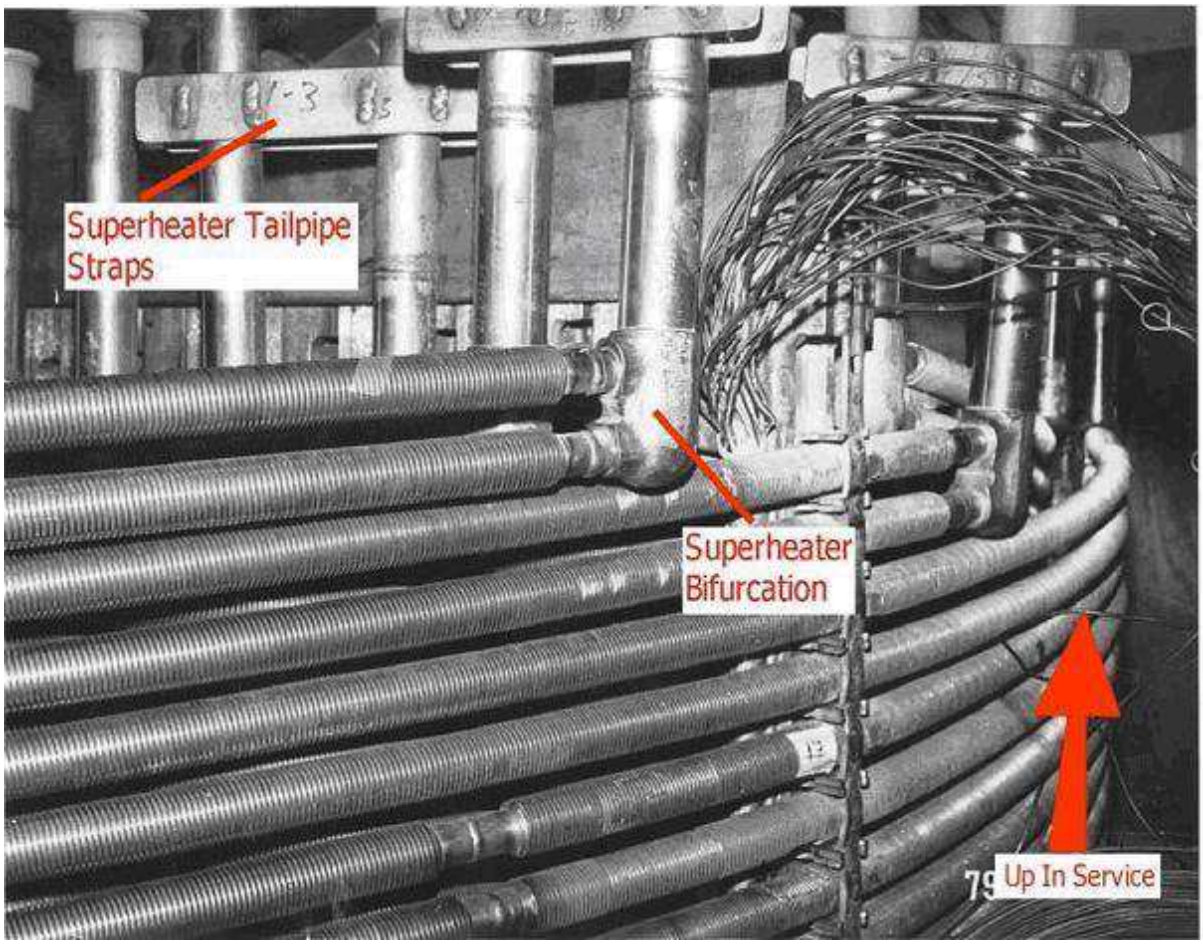

Fig.2. Illustrative unrestricted temperatures (MECT): first 15 years operation

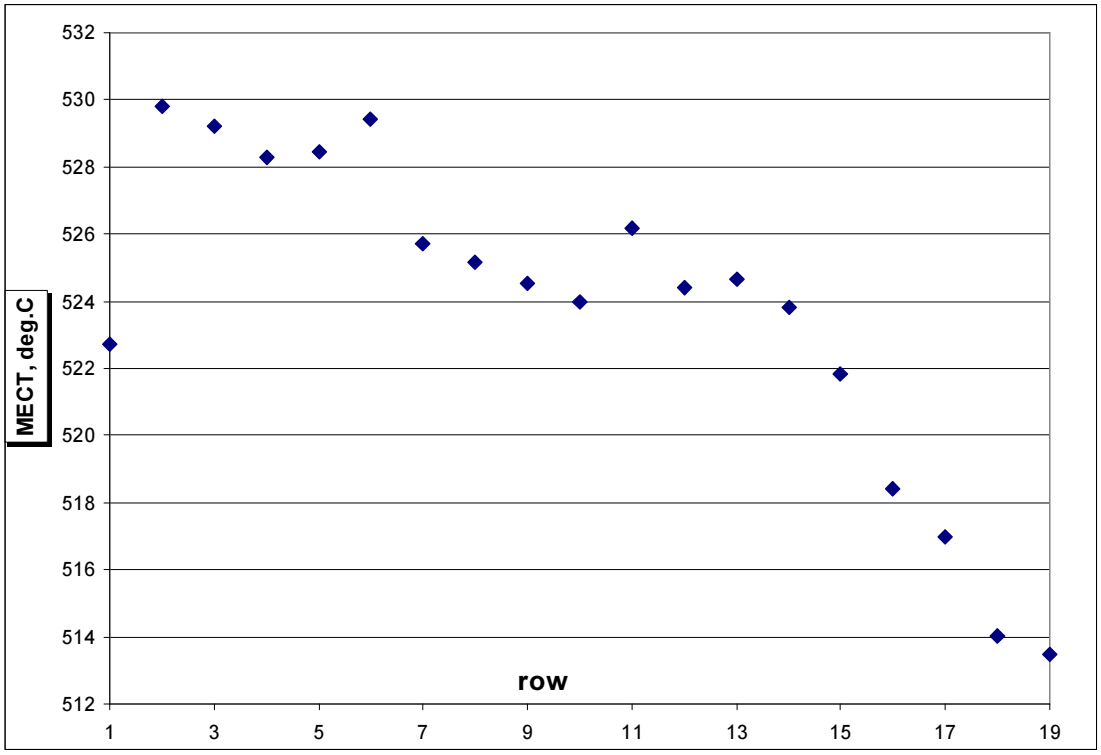

Fig.3. Illustrative tube temperature versus time for a highly restricted tube
The probabilistic program samples many such temperature-time curves for a given tube, this being the average for a particular tube.

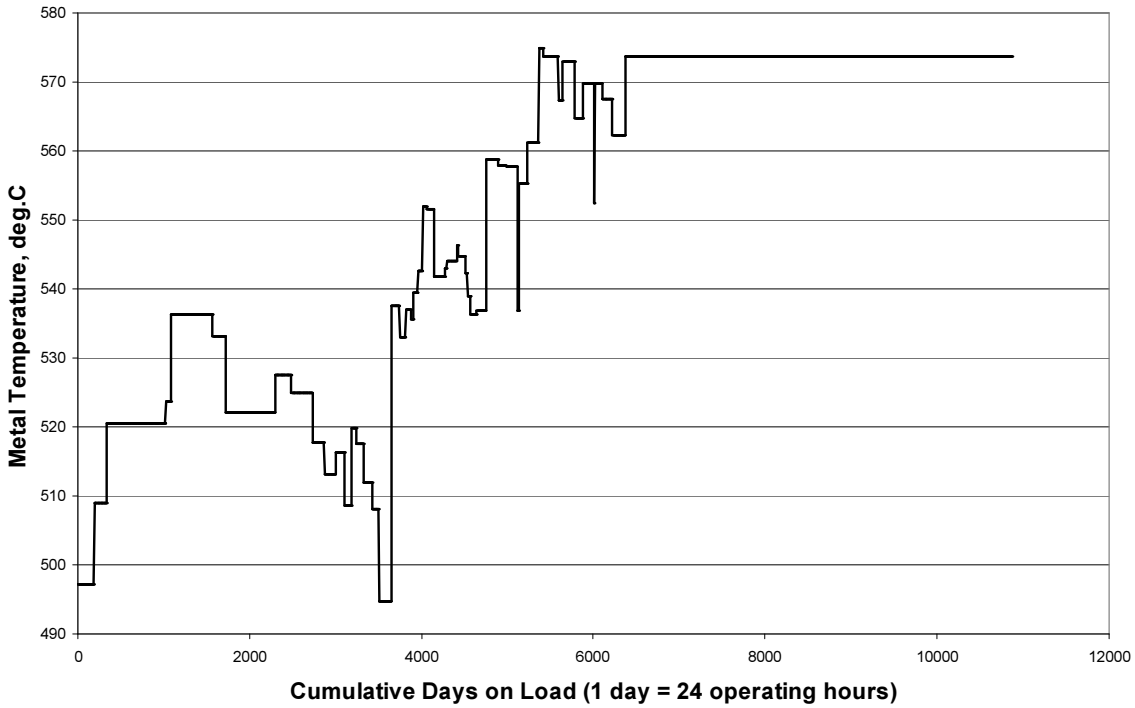

Fig.4. Illustrative wall thickness reduction over life (bounding restricted tube)

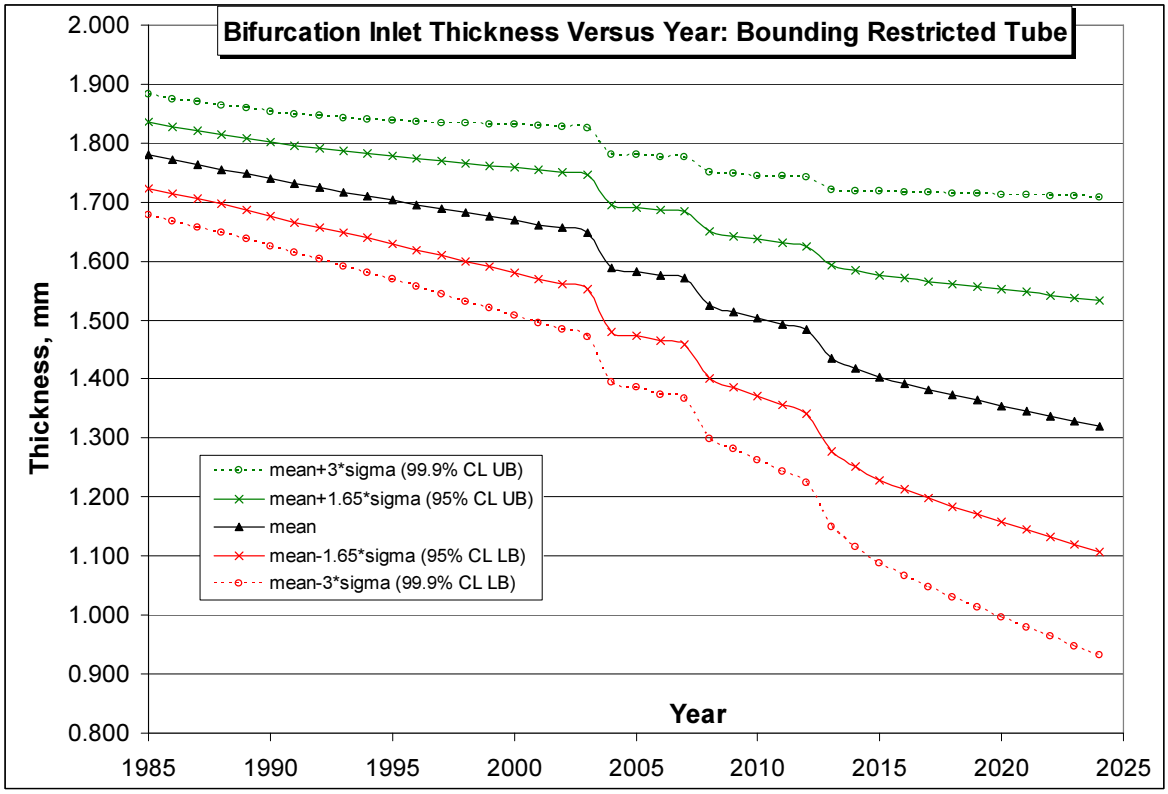

Fig.5. Dwell times for each of the 261 assessed cycles in order

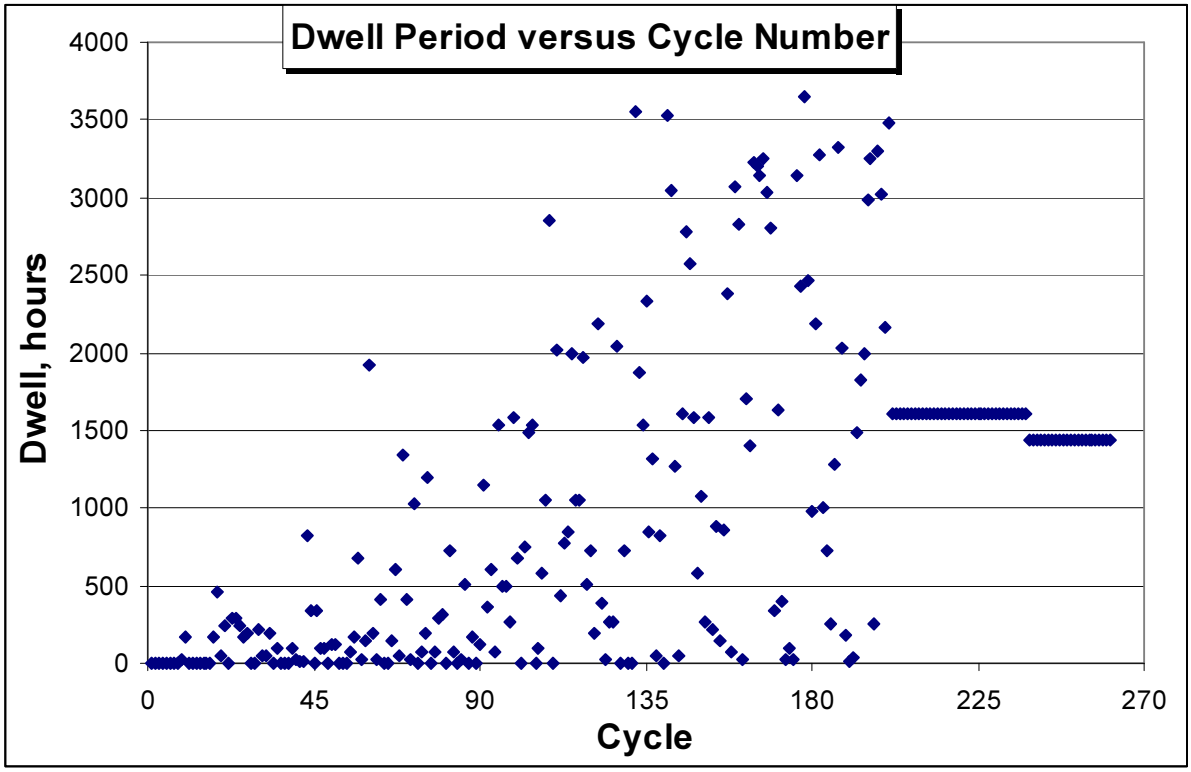

Fig.6. Overhang histogram

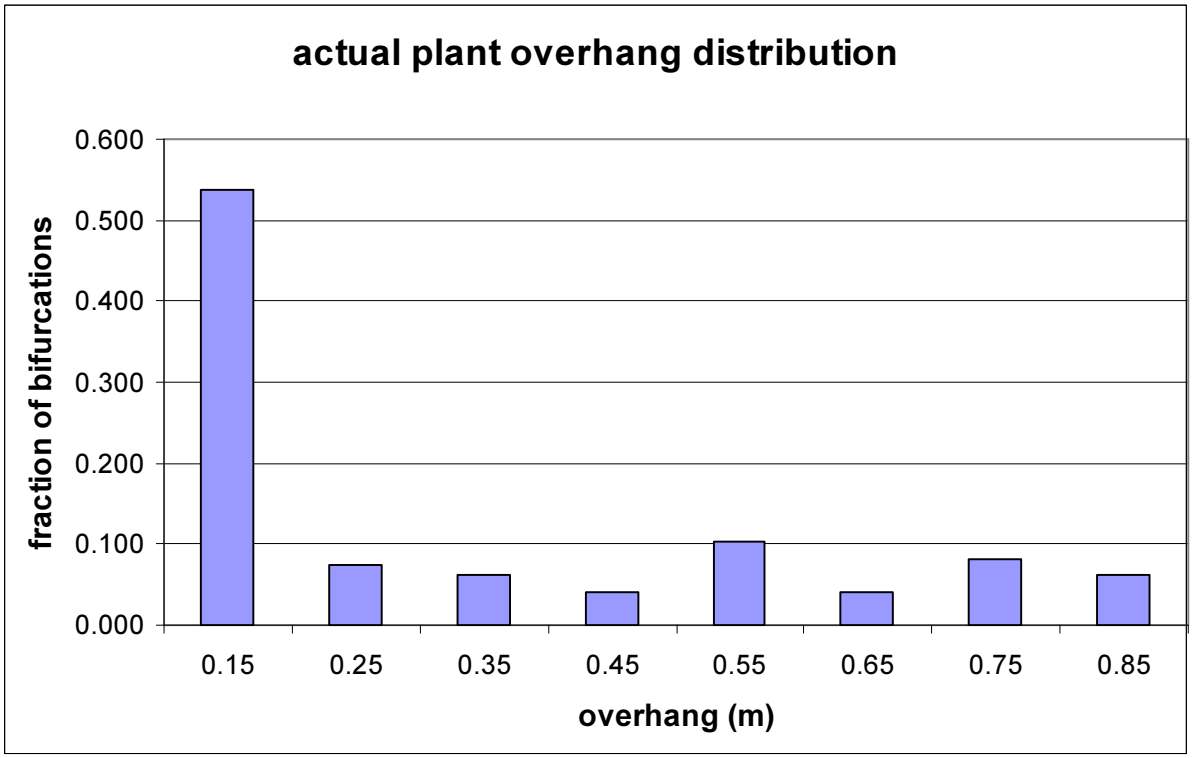

Fig.7. Reactor start-up transient thermal stress factors

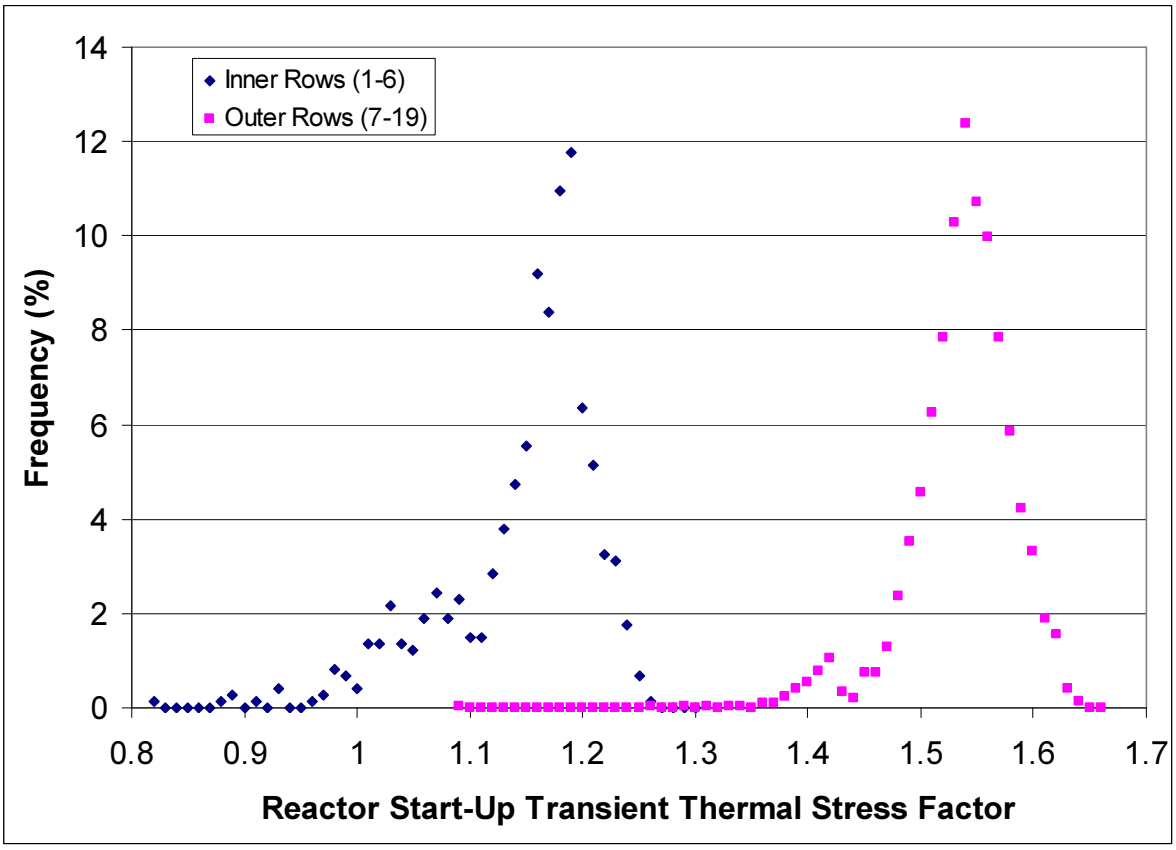

Fig.8. Reactor trip transient thermal stress factors

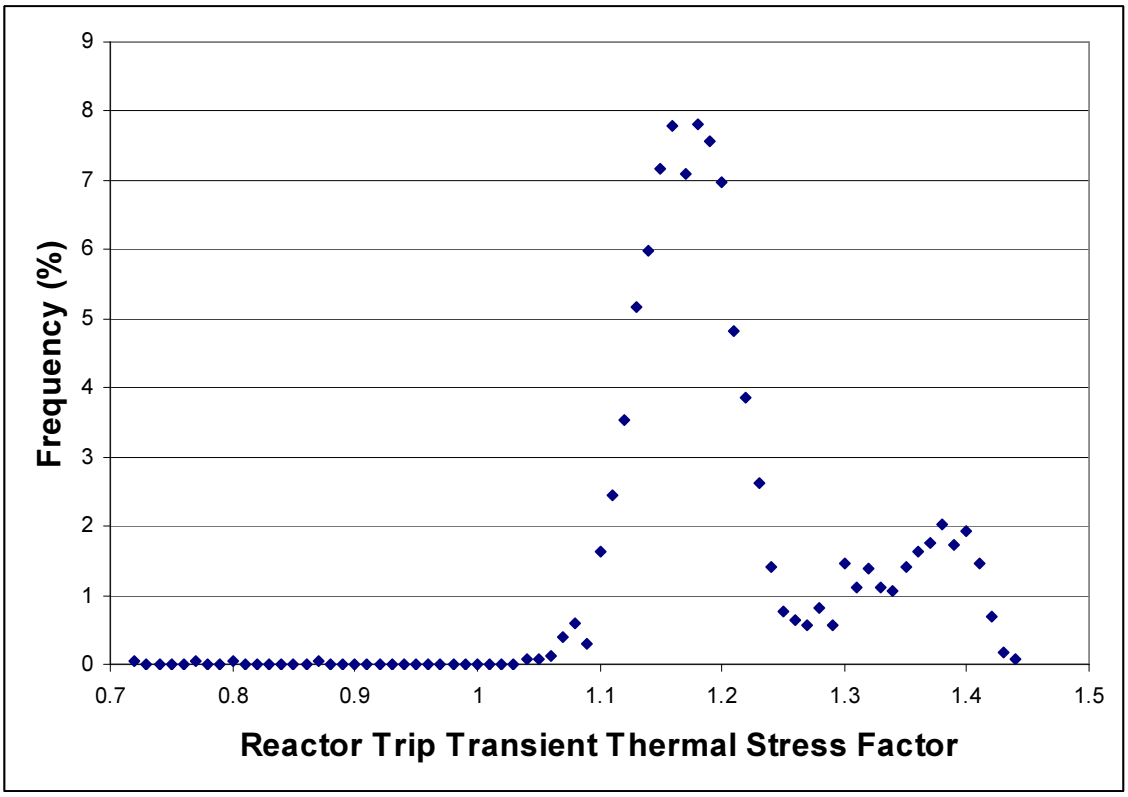

Fig.9. Histogram of minimum metal temperatures during hot standby

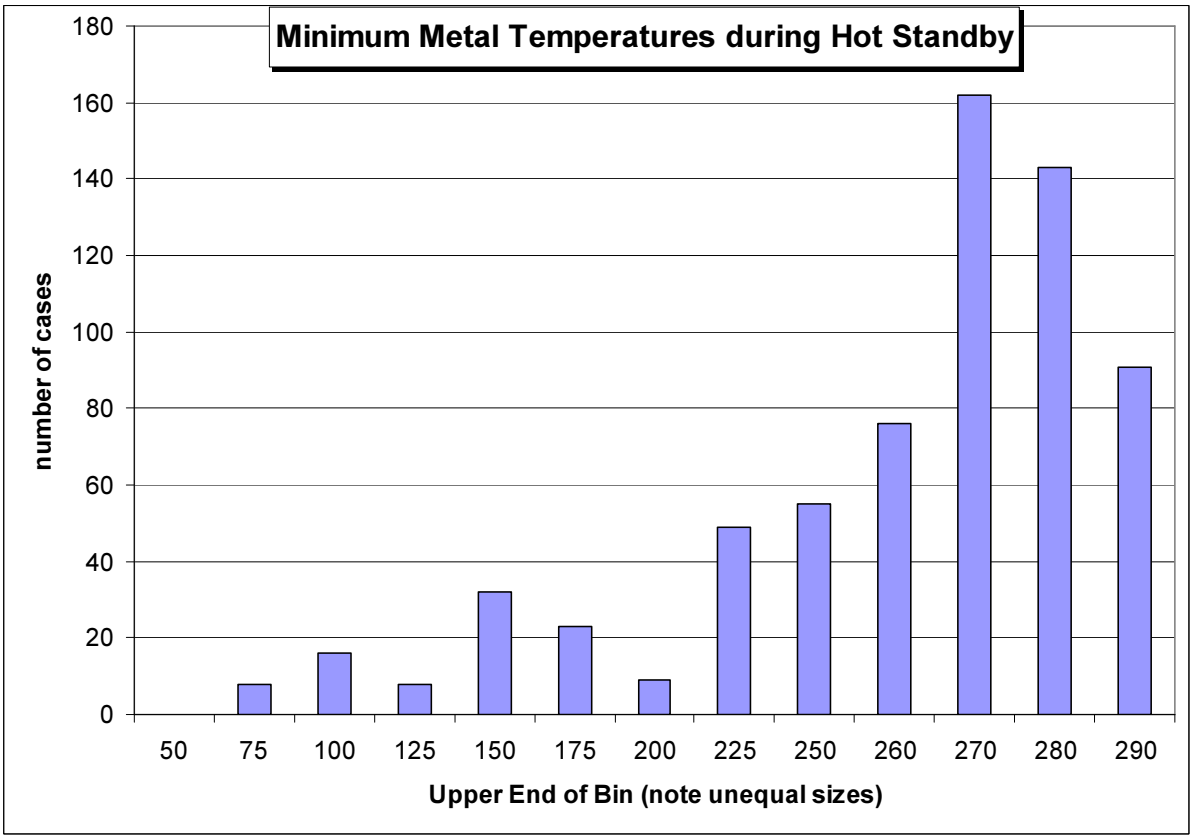

Fig.10. Sketch of idealised stress-strain hysteresis cycle

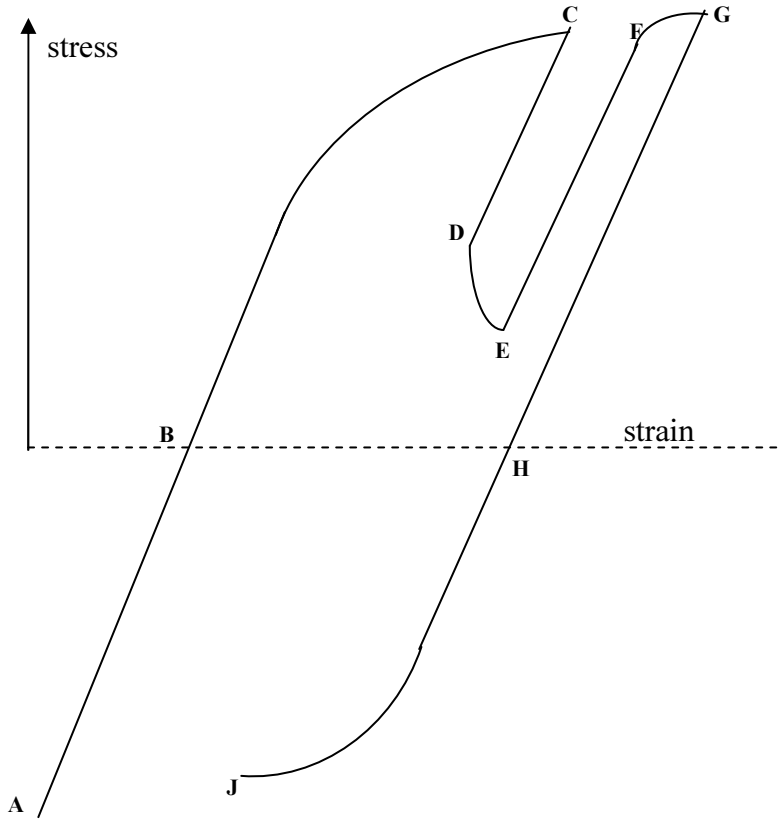

Fig.11. Example relaxation in the dwell of a creep-fatigue test on 316H material at 550°C: Minimum test stress versus calculated relaxed stress, continuous hardening and primary reset compared

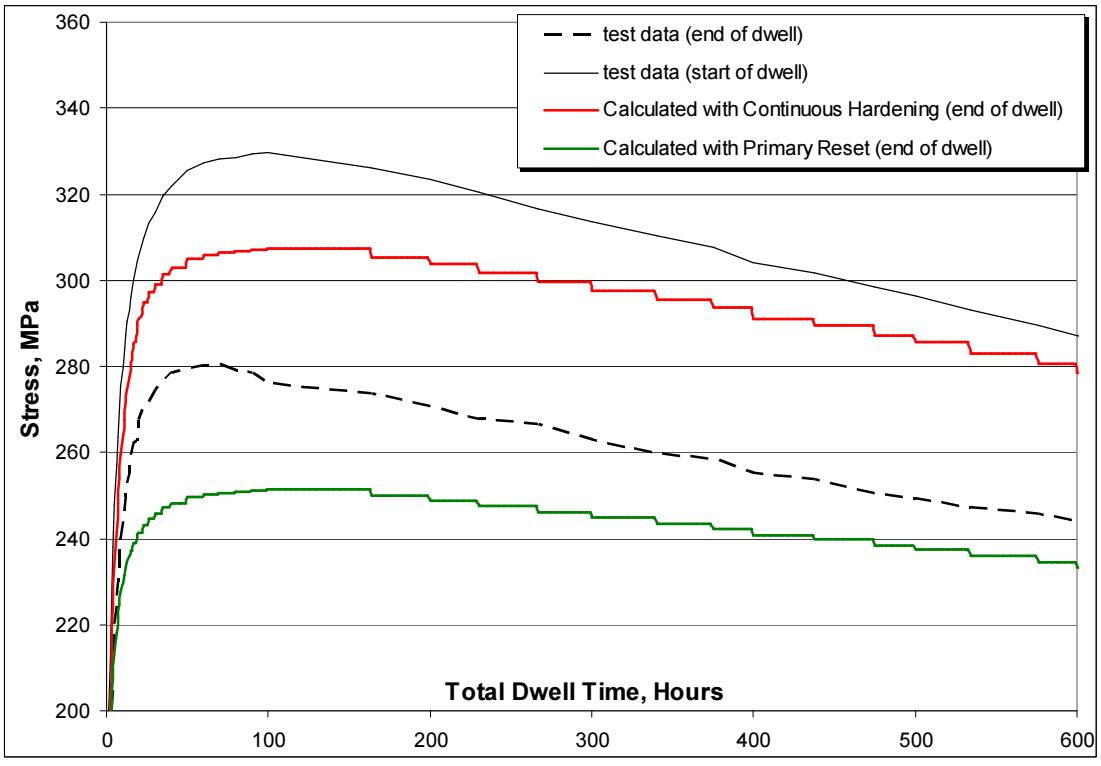

Fig.12. Convergence of crack initiation rate for restricted tubes (example)

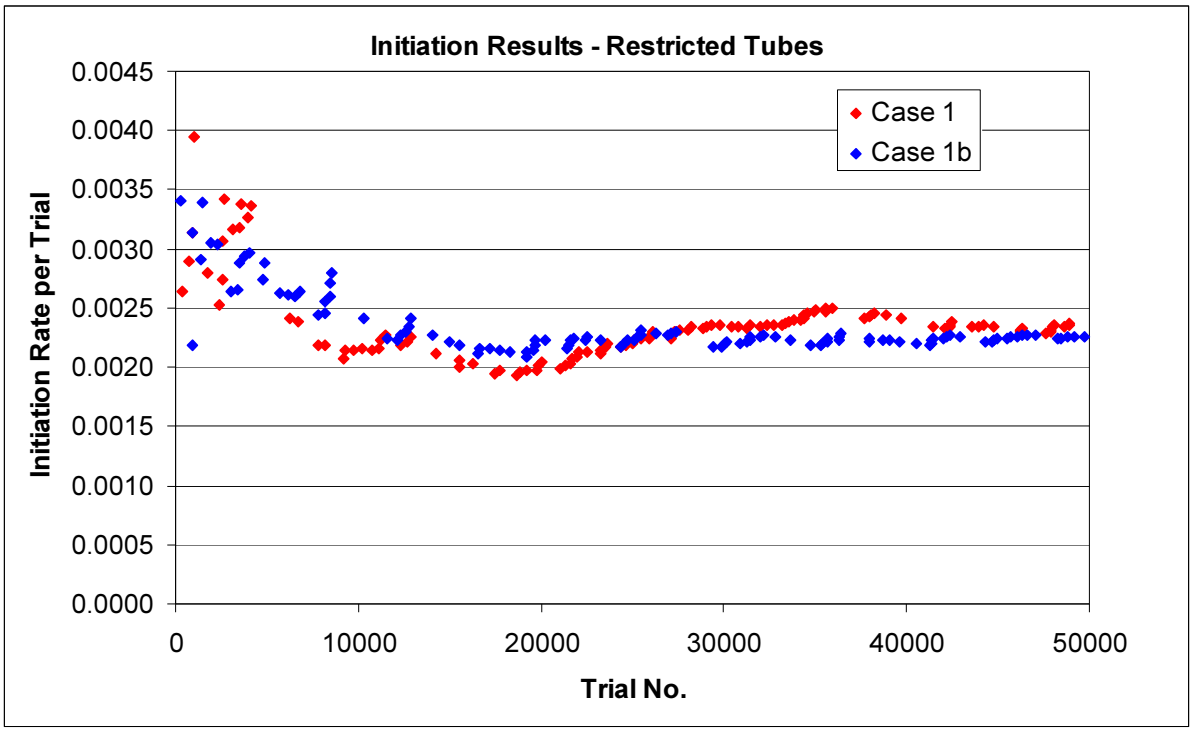

Fig.13. Future annual creep rupture probability per tube: Histogram over all 398 tubes with a restriction history. The annual failure probability plotted here is the average over the next 12 years of operation. The two "combinations" refer to different assumptions for the future restrictions.

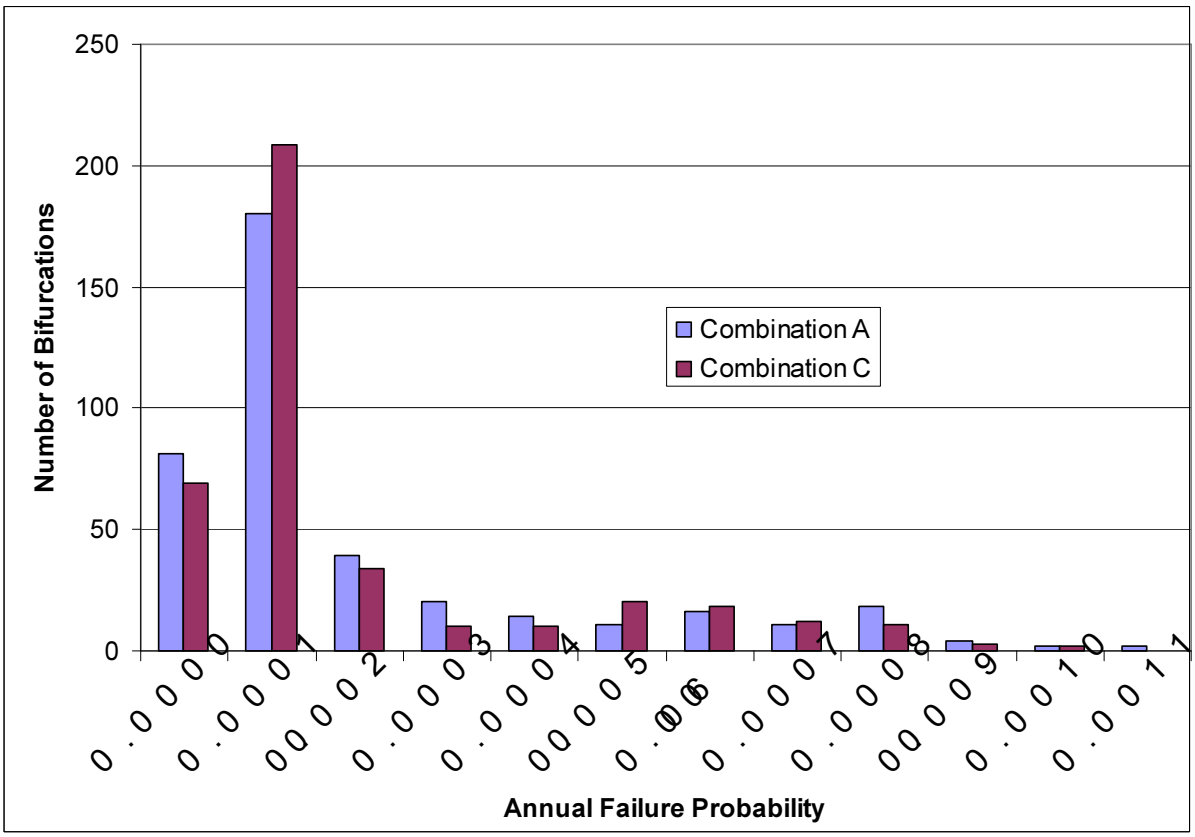

Fig.14. Future annual creep rupture probability per tube: Histogram over tubes with no restriction history. The annual failure probability plotted here is the average over the next 12 years of operation. The three different runs relate to different boilers.

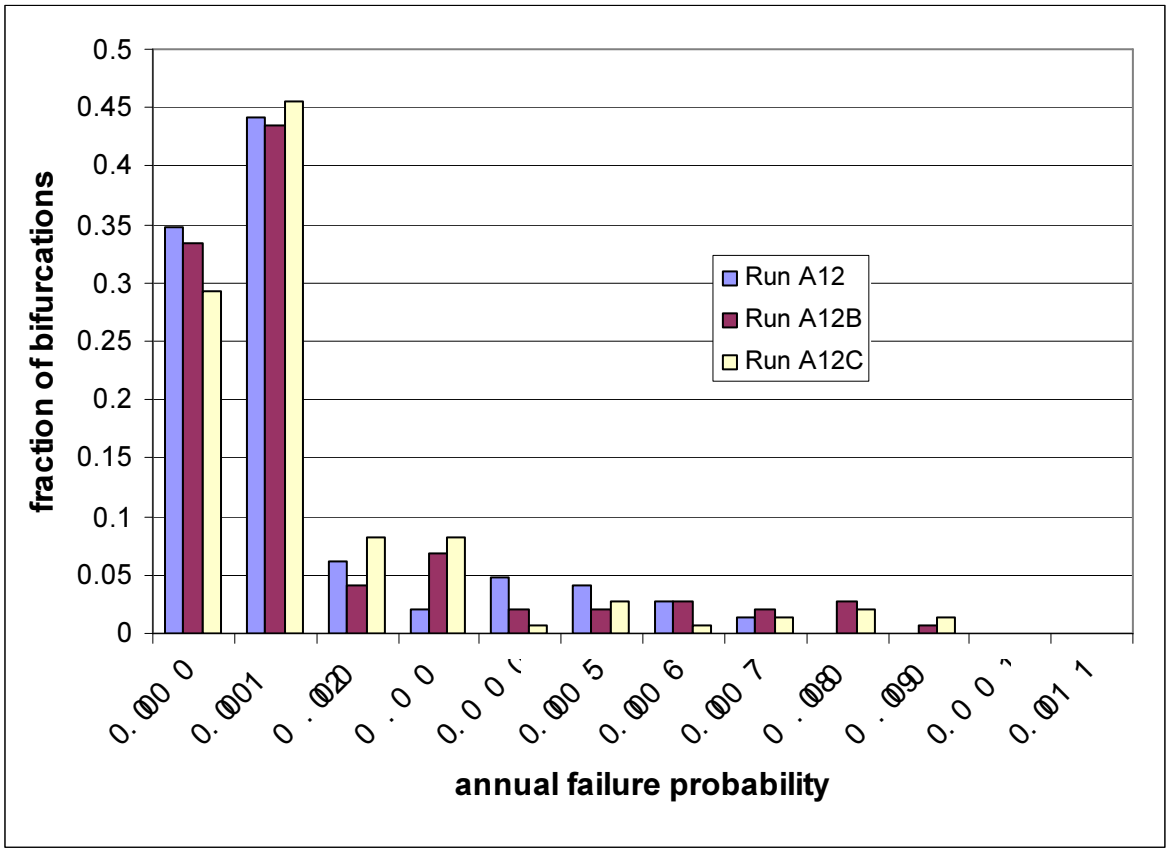

Fig.15. Annual creep rupture probability per tube versus year: Comparison of tubes with and without a restriction history.

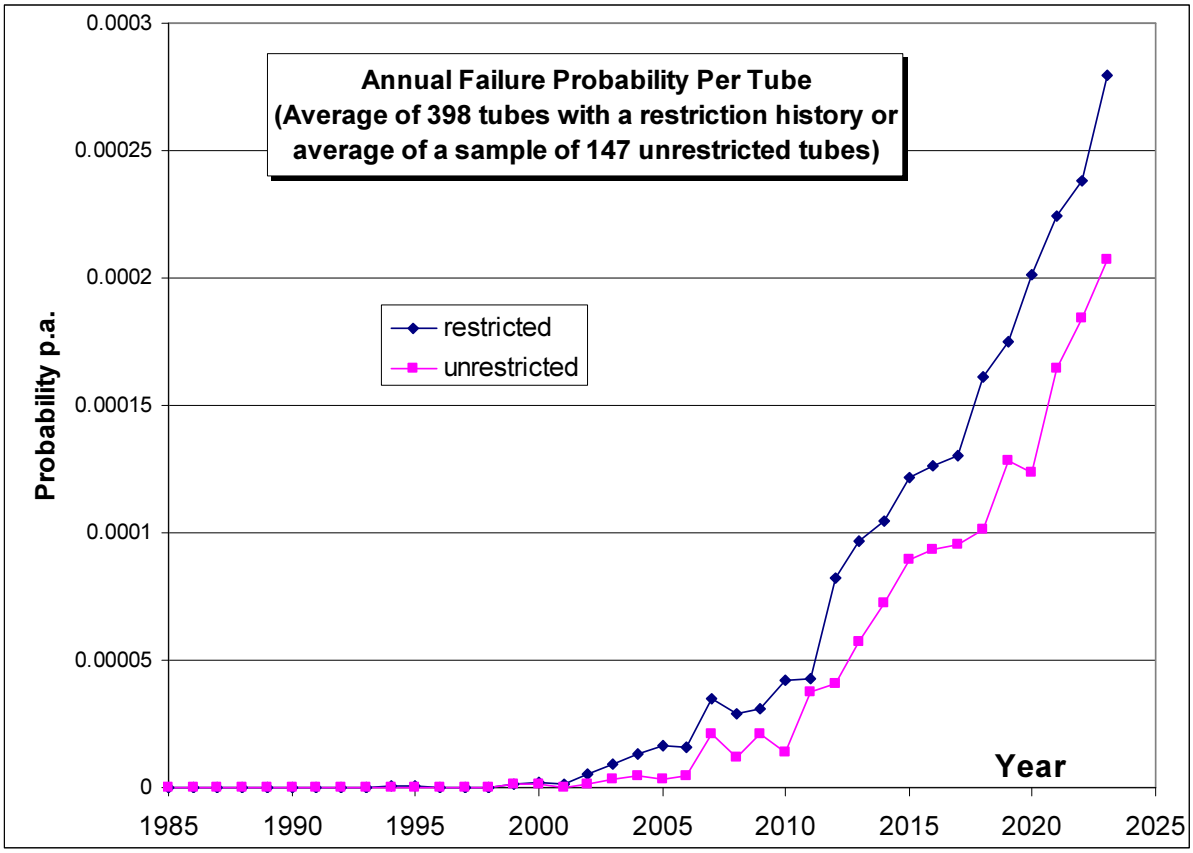

Fig.16. Illustration of creep damage due to welding residual stresses: Histogram of damage at the weld location over 3000 trials for the bounding restricted tube.

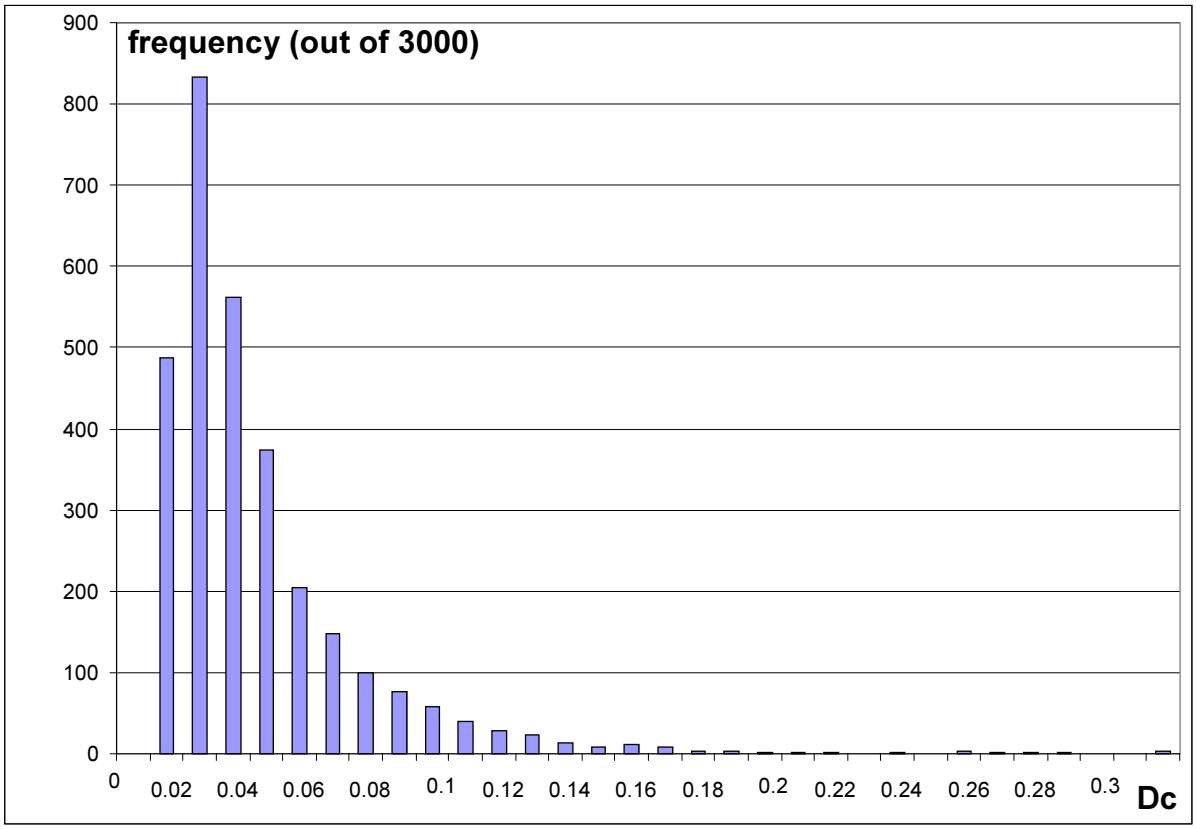

Fig.17. Predicted number of creep-fatigue crack initiations by the indicated operating hours

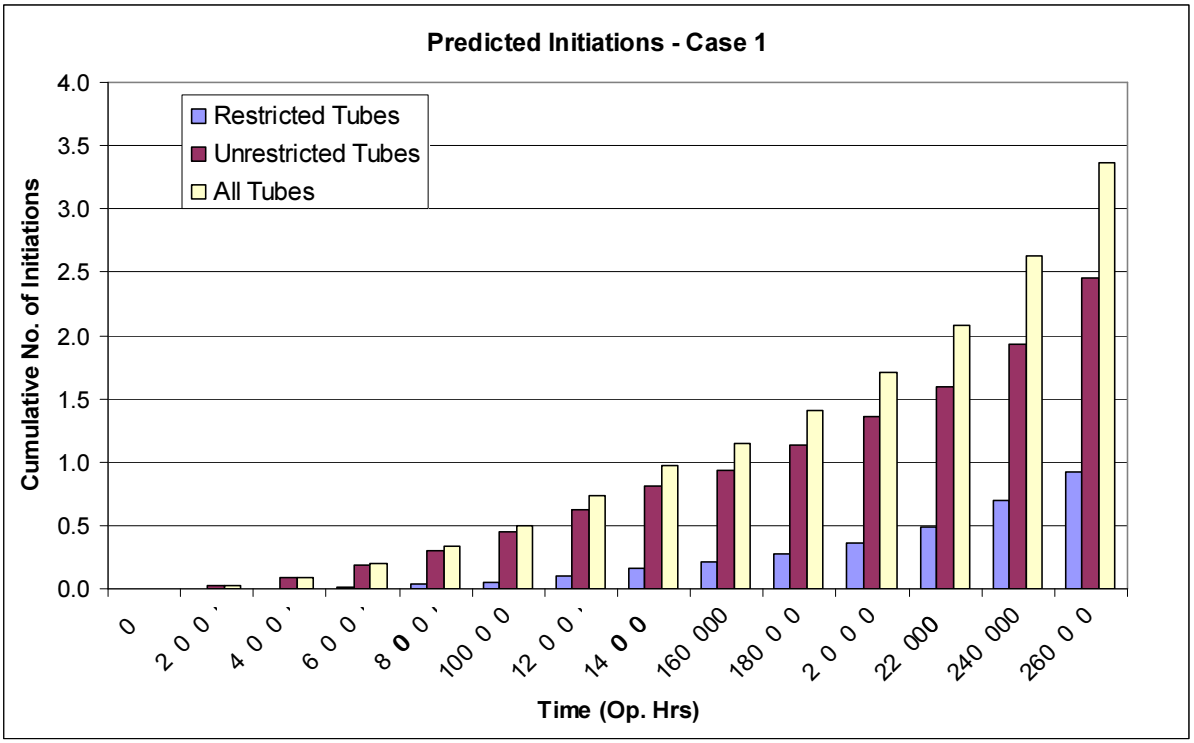

Fig.18. Histogram of percentage of dwells for which the start-of-dwell stress was set equal to the rupture reference stress: Unrestricted tubes

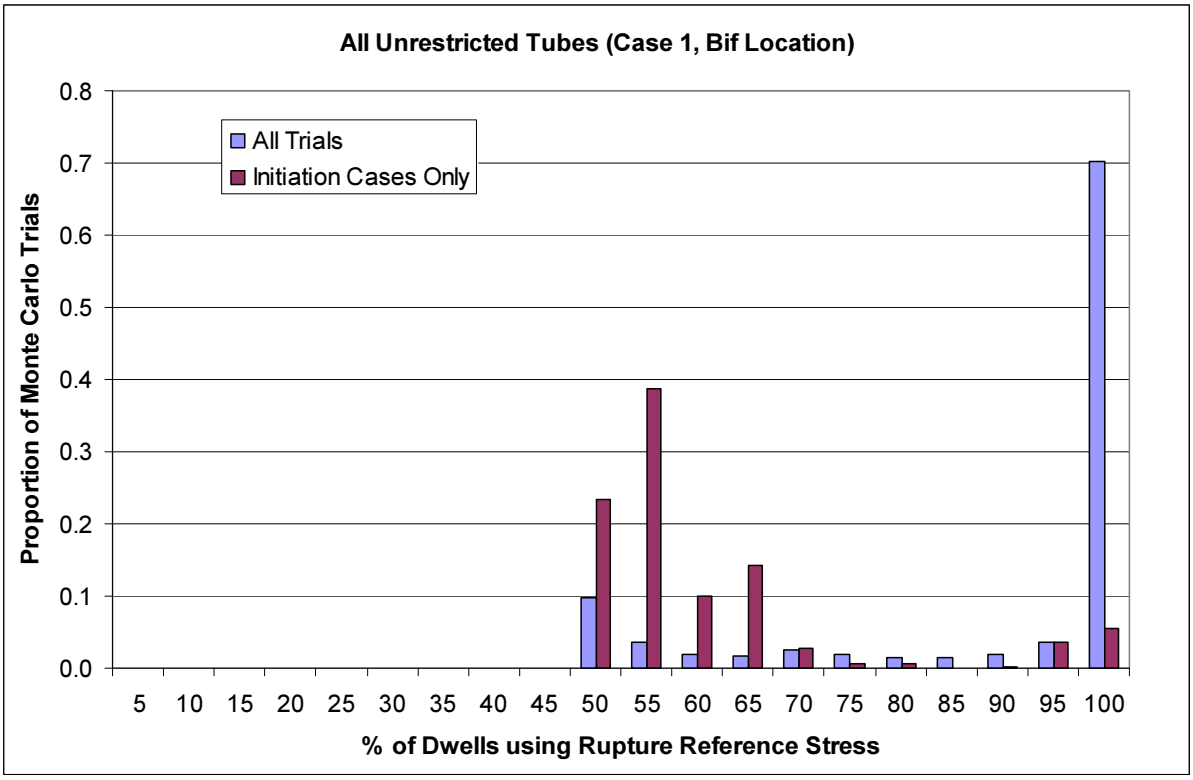

Fig.19. Histogram of percentage of dwells using primary creep reset: Unrestricted tubes